

Diffusion-GAN: Training GANs with Diffusion

Zhendong Wang¹, Huangjie Zheng^{1,2}, Pengcheng He², Weizhu Chen², and
Mingyuan Zhou¹

*{zhendong.wang, huangjie.zheng}@utexas.edu, {penhe,wzchen}@microsoft.com,
mingyuan.zhou@mcombs.utexas.edu*

¹The University of Texas at Austin

²Microsoft Azure AI

June 7, 2022

Abstract

For stable training of generative adversarial networks (GANs), injecting instance noise into the input of the discriminator is considered as a theoretically sound solution, which, however, has not yet delivered on its promise in practice. This paper introduces Diffusion-GAN that employs a Gaussian mixture distribution, defined over all the diffusion steps of a forward diffusion chain, to inject instance noise. A random sample from the mixture, which is diffused from an observed or generated data, is fed as the input to the discriminator. The generator is updated by backpropagating its gradient through the forward diffusion chain, whose length is adaptively adjusted to control the maximum noise-to-data ratio allowed at each training step. Theoretical analysis verifies the soundness of the proposed Diffusion-GAN, which provides model- and domain-agnostic differentiable augmentation. A rich set of experiments on diverse datasets show that Diffusion-GAN can provide stable and data-efficient GAN training, bringing consistent performance improvement over strong GAN baselines for synthesizing photo-realistic images.

1 Introduction

Generative adversarial networks (GANs) [Goodfellow et al., 2014] and their variants [Brock et al., 2018, Karras et al., 2019, 2020a, Zhao et al., 2020] have achieved great success in synthesizing photo-realistic images. GANs in practice, however, are known to suffer from a variety of issues ranging from non-convergence and training instability to mode collapse [Arjovsky and Bottou, 2017, Mescheder et al., 2018]. As a result, a wide array of analyses and modifications has been proposed for GANs, including improving the network architectures [Karras et al., 2019, Radford et al., 2016, Sauer et al., 2021, Zhang et al., 2019], gaining theoretical understanding of GAN training [Arjovsky and Bottou, 2017, Heusel et al., 2017, Mescheder et al., 2017, 2018], changing the objective function [Arjovsky et al., 2017, Bellemare et al., 2017, Deshpande et al., 2018, Li et al., 2017a, Nowozin et al., 2016, Zheng and Zhou, 2021], regularizing the weights and/or gradients [Arjovsky et al., 2017, Fedus et al., 2018, Mescheder et al., 2018, Miyato et al., 2018, Roth et al., 2017, Salimans et al., 2016], utilizing side information [Wang et al., 2018, Zhang et al., 2017, 2020b], adding a mapping from the data to latent representation [Donahue et al., 2016, Dumoulin et al., 2016, Li et al., 2017b], and applying data augmentation [Karras et al., 2020a, Zhang et al., 2020a, Zhao et al., 2020].

To stabilize GAN training, both Arjovsky and Bottou [2017] and Sønderby et al. [2017] suggest injecting instance noise, *i.e.*, adding noise to the input of the discriminator, as a simple way to broaden the support of both the generator and discriminator distributions and hence make the discriminator more resistant to overfitting. While its promise has been empirically verified in Sønderby et al. [2017] on image super-resolution and theoretically justified in Arjovsky and Bottou [2017], due to the difficulty to identify a suitable noise distribution, it is challenging to convert this idea into a practical solution for GAN training [Arjovsky and Bottou, 2017]. In particular, Roth et al. [2017] have shown in their experiments that naively adding instance noise to the high-dimensional input of the discriminator does not result in satisfactory performance. Instead, they propose to approximate the use of instance noise by adding a zero-centered gradient penalty on the discriminator. Both theoretical and empirical justifications on the convergence of this approach can be found in Mescheder et al. [2018], whose experimental results show that adding zero-centered gradient penalties to non-saturating GANs leads to stable training, providing better or comparable generation performance in comparison to Wasserstein GANs with gradient penalty (WGAN-GP) [Arjovsky et al., 2017]. However, as shown in Brock et al. [2018], cautions should be made when applying zero-centered gradient penalties and several other related regularization strategies, as while they could help achieve stable training, they may also clearly hurt the generation performance.

To inject proper instance noise that can facilitate GAN training, we propose Diffusion-GAN that does so with a diffusion-based Gaussian mixture distribution. A graphical illustration of Diffusion-GAN is shown in Figure 1. For the diffusion process in Diffusion-GAN, the input is the real or generated data, the length of the diffusion chain is adaptively adjusted, and a sample drawn from a Gaussian mixture distribution defined over all the diffusion steps is fed as the input to the discriminator. Moreover, the forward diffusion chain is set to be differentiable at all its diffusion steps so that the gradient can be back-propagated through it and then the discriminator to update the generator. Comparing to vanilla GANs which feed the original observed and generated images to the discriminator, Diffusion-GAN corrupts these images with instance noise before feeding them to the discriminator. Different from naively adding an instance noise following a specific distribution to corrupt the images, Diffusion-GAN introduces a diffusion-based Gaussian mixture distribution, whose mixture components take weighted combinations of the images and noise at various noise-to-data ratios. This novel solution provides not only training stability but also domain-agnostic differentiable data augmentation that enhances data efficiency. We provide theoretical analysis to show that when the discriminator is optimized, the divergence corresponding to the min-max objective of Diffusion-GAN is continuous and differentiable everywhere, providing useful gradient for the generator even when the data and generator distributions have disjoint supports, which is known to cause issues in GAN training.

Our main contributions include: 1) We propose Diffusion-GAN that employs a forward diffusion-based mixture distribution to inject instance noise to achieve stable data-efficient GAN training; 2) We provide theoretical analysis showing that the objective function of Diffusion-GAN is well defined even when the data and generator distributions have non-overlapping supports; 3) We conduct extensive experiments on a variety of toy and real datasets, which show that Diffusion-GAN provides model- and domain-agnostic differentiable augmentation for data-efficient GAN training, boosting the stability and generation performance of strong baselines, including StyleGAN2 [Karras et al., 2020b] and Projected GAN [Sauer et al., 2021], as well as achieving state-of-the-art results in synthesizing high-resolution photo-realistic images, as measured by both the Fréchet Inception Distance (FID) [Heusel et al., 2017] and Recall score [Kynkäänniemi et al., 2019].

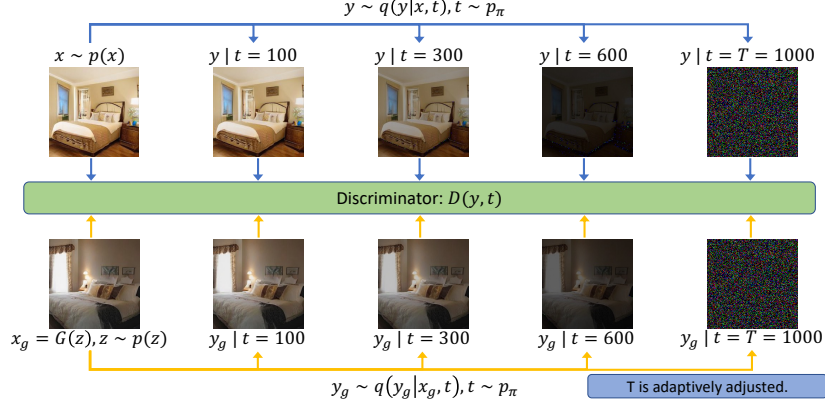


Figure 1: Flowchart for Diffusion-GAN. The top row images represent the forward diffusion process of a real image, while the bottom row images represent the forward diffusion process of a generated fake image. The discriminator learns to distinguish a diffused real image from a diffused fake image at all diffusion steps.

2 Training GANs with diffusion-based mixture distribution

Below we first briefly review GANs and diffusion models and then present our method and analyze its theoretical properties. GANs aim to model data distribution $p(\mathbf{x})$ via a min-max game played between a generator and a discriminator [Goodfellow et al., 2014]. The generator G aims to transform noise \mathbf{z} into $G(\mathbf{z})$ that mimics real data, while the discriminator D learns to distinguish the generated samples $G(\mathbf{z})$ from real ones $\mathbf{x} \sim p(\mathbf{x})$. The min-max objective of GANs can be expressed as

$$\min_G \max_D V(G, D) = \mathbb{E}_{\mathbf{x} \sim p(\mathbf{x})} [\log(D(\mathbf{x}))] + \mathbb{E}_{\mathbf{z} \sim p(\mathbf{z})} [\log(1 - D(G(\mathbf{z})))] \quad (1)$$

While in practice this vanilla objective is often modified in a certain way [Goodfellow et al., 2014, Miyato et al., 2018, Fedus et al., 2018], the use of adversarial learning between G and D in general remains intact.

Diffusion-based generative models [Ho et al., 2020, Sohl-Dickstein et al., 2015, Song and Ermon, 2019] assume $p_\theta(\mathbf{x}_0) := \int p_\theta(\mathbf{x}_{0:T}) d\mathbf{x}_{1:T}$, where $\mathbf{x}_1, \dots, \mathbf{x}_T$ are latent variables of the same dimensionality as the data $\mathbf{x}_0 \sim p(\mathbf{x}_0)$. There is a forward diffusion chain that gradually adds noise to the data $\mathbf{x}_0 \sim q(\mathbf{x}_0)$ in T steps with pre-defined variance schedule β_t and variance σ^2 :

$$q(\mathbf{x}_{1:T} | \mathbf{x}_0) := \prod_{t=1}^T q(\mathbf{x}_t | \mathbf{x}_{t-1}), \quad q(\mathbf{x}_t | \mathbf{x}_{t-1}) := \mathcal{N}(\mathbf{x}_t; \sqrt{1 - \beta_t} \mathbf{x}_{t-1}, \beta_t \sigma^2 \mathbf{I}). \quad (2)$$

A notable property is that \mathbf{x}_t at an arbitrary time-step t can be sampled in closed form as

$$q(\mathbf{x}_t | \mathbf{x}_0) = \mathcal{N}(\mathbf{x}_t; \sqrt{\bar{\alpha}_t} \mathbf{x}_0, (1 - \bar{\alpha}_t) \sigma^2 \mathbf{I}), \quad \text{where } \alpha_t := 1 - \beta_t, \quad \bar{\alpha}_t := \prod_{s=1}^t \alpha_s. \quad (3)$$

A reverse diffusion chain, constructed as

$$p_\theta(\mathbf{x}_{0:T}) := \mathcal{N}(\mathbf{x}_T; \mathbf{0}, \sigma^2 \mathbf{I}) \prod_{t=1}^T p_\theta(\mathbf{x}_{t-1} | \mathbf{x}_t), \quad (4)$$

is then optimized with the evidence lower bound [Jordan et al., 1999, Blei et al., 2017] as $\mathbb{E}_q[\ln \frac{p_\theta(\mathbf{x}_{0:T})}{q(\mathbf{x}_{1:T} | \mathbf{x}_0)}]$.

2.1 Instance noise injection via a diffusion-based mixture distribution

Let $\mathbf{z} \sim p(\mathbf{z})$ denote the latent variable distribution and $p_g(\mathbf{x})$ denote the distribution of $\mathbf{x}_g = G(\mathbf{z})$. We inject instance noise through a forward diffusion chain-based mixture distribution as

$$\mathbf{x} \sim p(\mathbf{x}), \mathbf{y} \sim q(\mathbf{y} | \mathbf{x}), \quad q(\mathbf{y} | \mathbf{x}) := \sum_{t=1}^T \pi_t q(\mathbf{y} | \mathbf{x}, t), \quad (5)$$

$$\mathbf{x}_g \sim p_g(\mathbf{x}), \mathbf{y}_g \sim q(\mathbf{y}_g | \mathbf{x}_g), \quad q(\mathbf{y}_g | \mathbf{x}_g) := \sum_{t=1}^T \pi_t q(\mathbf{y}_g | \mathbf{x}_g, t), \quad (6)$$

where $q(\mathbf{y} | \mathbf{x})$ is a T -component mixture distribution, the mixture weights π_t are non-negative and sum to one, and the mixture components $q(\mathbf{y} | \mathbf{x}, t)$ are obtained via diffusion as in (3), expressed as

$$q(\mathbf{y} | \mathbf{x}, t) = \mathcal{N}(\mathbf{y}; \sqrt{\bar{\alpha}_t} \mathbf{x}, (1 - \bar{\alpha}_t) \sigma^2 \mathbf{I}). \quad (7)$$

Samples from this mixture can be drawn as $t \sim p_\pi := \text{Discrete}(\pi_1, \dots, \pi_T)$, $\mathbf{y} \sim q(\mathbf{y} | \mathbf{x}, t)$. Under this construction, $q(\mathbf{y} | \mathbf{x}, t)$ becomes the marginal distribution of \mathbf{x} after going through the forward diffusion chain t steps, and $q(\mathbf{y} | \mathbf{x})$ becomes a Gaussian mixture distribution that involves all T steps of the diffusion chain. We note the larger the t is, the stronger the noise is injected into $\mathbf{y} \sim q(\mathbf{y} | \mathbf{x}, t)$ and the weaker the data becomes. A simple choice for p_π is to let $\pi_t = 1/T$ for all t . Below we will discuss a different choice that favors sampling a larger t and hence a larger noise-to-data ratio. Next we introduce Diffusion-GAN that trains its discriminator and generator with the help of the diffusion-induced mixture distribution.

The Diffusion-GAN’s counterpart to the vanilla GAN min-max objective is defined as

$$V(G, D) = \mathbb{E}_{\mathbf{x} \sim p(\mathbf{x}), t \sim p_\pi, \mathbf{y} \sim q(\mathbf{y} | \mathbf{x}, t)} [\log(D_\phi(\mathbf{y}, t))] + \mathbb{E}_{\mathbf{z} \sim p(\mathbf{z}), t \sim p_\pi, \mathbf{y}_g \sim q(\mathbf{y}_g | G_\theta(\mathbf{z}), t)} [\log(1 - D_\phi(\mathbf{y}_g, t))]. \quad (8)$$

The discriminator D learns to distinguish the diffused generated samples \mathbf{y}_g from the diffused real observations \mathbf{y} for $\forall t \in \{1, \dots, T\}$, with specific priorities determined by the values of π_t . The generator G learns to map a latent variable \mathbf{z} to its output $\mathbf{x}_g = G_\theta(\mathbf{z})$, which can fool the discriminator at any step of the diffusion chain. Since $\mathbf{y}_g \sim q(\mathbf{y}_g | G_\theta(\mathbf{z}), t)$ can be reparameterized as $\mathbf{y}_g = \sqrt{\bar{\alpha}_t} G_\theta(\mathbf{z}) + \sqrt{(1 - \bar{\alpha}_t)} \sigma \boldsymbol{\epsilon}$, $\boldsymbol{\epsilon} \sim \mathcal{N}(0, \mathbf{I})$, the gradient computed on Equation (8) can be backpropagated to the generator directly. Similar to Goodfellow et al. [2014], one can show that the adversarial loss in Equation (8) approximately minimizes the *Jensen–Shannon (JS) divergence*,

$$\mathcal{D}_{\text{JS}}(p(\mathbf{y}, t) || p_g(\mathbf{y}, t)) = \mathbb{E}_{t \sim p_\pi} [\mathcal{D}_{\text{JS}}(p(\mathbf{y} | t) || p_g(\mathbf{y} | t))]. \quad (9)$$

The derivation of the equality in Equation (9) is provided in Appendix B. One critical question is whether minimizing $\mathcal{D}_{\text{JS}}(p(\mathbf{y}, t) || p_g(\mathbf{y}, t))$ induces the same optimal generator as minimizing the original $\mathcal{D}_{\text{JS}}(p(\mathbf{x}) || p_g(\mathbf{x}))$. We will theoretically show that the answer is yes in Section 2.3.

2.2 Adaptiveness of diffusion

Note that as t increases, $\bar{\alpha}_t$ decreases towards zero and hence the noise-to-data ratios in both \mathbf{y} and \mathbf{y}_g increase, inducing a more and more difficult task for the discriminator D . Since GANs are known to suffer from the discriminator overfitting issue [Karras et al., 2020a, Zhao et al., 2020], we design an adaptive control of the diffusion intensity so as to better train the discriminator. We achieve this by adaptively modifying T .

Ideally we want the discriminator to start with the original data samples, and as the discriminator becomes more confident, we feed it with harder samples from a larger t . Thus, we design a self-paced schedule for T based on a metric r_d , which evaluates the overfitting of the discriminator:

$$r_d = \mathbb{E}_{\mathbf{y}, t \sim p(\mathbf{y}, t)} [\text{sign}(D_\phi(\mathbf{y}, t) - 0.5)], \quad T = T + \text{sign}(r_d - d_{\text{target}}) * C \quad (10)$$

where r_d follows the choice of Karras et al. [2020a] and C is a fixed constant. We evaluate r_d every four minibatches and update T at the same time. To better resist discriminator overfitting, we define

$$t \sim p_\pi := \text{Discrete} \left(\frac{1}{\sum_{t=1}^T t}, \frac{2}{\sum_{t=1}^T t}, \dots, \frac{T}{\sum_{t=1}^T t} \right) \quad (11)$$

as an asymmetric discrete distribution, which encourages the discriminator to observe newly added diffusion samples as T increases. This is because when T begins to increase, it implies the discriminator has already been confident about the seen samples so we want it to explore more new samples to counteract discriminator overfitting. Note that as $q(\mathbf{y} | \mathbf{x})$ is a Gaussian mixture defined over all steps of the diffusion chain, while the use of $\pi_t := t / \sum_{s=1}^T s$ favors a larger t , there is still a large probability to traverse small t . To smooth the change of T during training, we sample an exploration t list \mathbf{t}_{expl} from p_π , fix \mathbf{t}_{expl} during the update interval of T , and then sample t from \mathbf{t}_{expl} for augmenting data samples. This drives the model to explore every t sufficiently before querying to increment T . We summarize training Diffusion-GAN in Algorithm 1 in Appendix F.

2.3 Theoretical analysis

We provide two theorems, whose proofs are provided in Appendix A, to answer the following two questions: **(a)** Whether the diffusion-based instance noise injection helps ease the training of GANs? **(b)** Whether minimizing $\mathcal{D}_{\text{JS}}(p(\mathbf{y}, t) || p_g(\mathbf{y}, t))$ induces the same optimal generator as minimizing $\mathcal{D}_{\text{JS}}(p(\mathbf{x}) || p_g(\mathbf{x}))$? First to address **(a)**, we show that in general case the f -divergence [Nowozin et al., 2016] between $q(\mathbf{y} | t)$ and $q(\mathbf{y}_g | t)$, which are the marginal distributions of diffused samples at step t , is continuous and differentiable everywhere. Note that the JS divergence is a special case of f -divergence.

Theorem 1 (Gradient backpropagation through diffusion chain). *Let $p(\mathbf{x})$ be a fixed distribution over \mathcal{X} and \mathbf{z} be a random noise over another space \mathcal{Z} . Denote $G_\theta : \mathcal{Z} \rightarrow \mathcal{X}$ as a function with parameter θ and input \mathbf{z} and $p_g(\mathbf{x})$ as the distribution of $G_\theta(\mathbf{z})$. Let $q(\mathbf{y} | \mathbf{x}, t) = \mathcal{N}(\mathbf{y}; \sqrt{\bar{\alpha}_t} \mathbf{x}, (1 - \bar{\alpha}_t) \sigma^2 \mathbf{I})$, where $\bar{\alpha}_t \in (0, 1)$ and $\sigma > 0$. Let $q(\mathbf{y} | t) = \int p(\mathbf{x}) q(\mathbf{y} | \mathbf{x}, t) d\mathbf{x}$ and $q_g(\mathbf{y} | t) = \int p_g(\mathbf{x}) q(\mathbf{y} | \mathbf{x}, t) d\mathbf{x}$. Then, $\forall t$, if function G_θ is continuous and differentiable, the f -divergence $\mathcal{D}_f(q(\mathbf{y} | t) || q_g(\mathbf{y} | t))$ is continuous and differentiable with respect to θ .*

Theorem 2 (Non-leaking data augmentation). *Let $\mathbf{x} \sim p(\mathbf{x})$, $\mathbf{y} \sim q(\mathbf{y} | \mathbf{x})$ and $\mathbf{x}_g \sim p_g(\mathbf{x})$, $\mathbf{y}_g \sim q(\mathbf{y}_g | \mathbf{x}_g)$, where $q(\mathbf{y} | \mathbf{x})$ is the transition density. Given certain $q(\mathbf{y} | \mathbf{x})$, if \mathbf{y} could be reparameterized into $\mathbf{y} = f(\mathbf{x}) + h(\boldsymbol{\epsilon})$, $\boldsymbol{\epsilon} \sim p(\boldsymbol{\epsilon})$, where $p(\boldsymbol{\epsilon})$ is a known distribution, and both f and h are one-to-one mapping functions, then we could have $p(\mathbf{y}) = p_g(\mathbf{y}) \Leftrightarrow p(\mathbf{x}) = p_g(\mathbf{x})$.*

Theorem 1 shows that with the help of diffusion noise injection by $q(\mathbf{y} | \mathbf{x}, t)$, $\forall t$, \mathbf{y} and \mathbf{y}_g are defined on the same support space, the whole \mathcal{X} , and $\mathcal{D}_f(q(\mathbf{y} | t) || q_g(\mathbf{y} | t))$ is continuous and differentiable everywhere. Note that if $q(\mathbf{y})$ and $q_g(\mathbf{y})$ are far away from each other and t is not sufficiently large, $\mathcal{D}_f(q(\mathbf{y} | t) || q_g(\mathbf{y} | t))$ could still keep a near constant value and hence provide little useful gradient. However, as $t \sim \text{Discrete}(\pi_1, \dots, \pi_T)$, there is always a good chance that a sufficiently large t is sampled to provide useful gradient. We empirically show this through a toy example in Section 4. By Theorem 2, if we take $\mathbf{y} | t$ as the \mathbf{y} introduced in the theorem, then $\forall t$, Equation (3) fits the assumption made on $q(\mathbf{y} | \mathbf{x})$ and hence minimizing $\mathcal{D}_f(q(\mathbf{y} | t) || q_g(\mathbf{y} | t))$ has the same ultimate effect of minimizing the original $\mathcal{D}_f(p(\mathbf{x}) || p_g(\mathbf{x}))$, which suggests that there is no need to worry about leaking noise injection into the generated samples.

3 Related work

Stabilizing GAN training. A root cause of training difficulties in GANs is often attributed to the JS divergence that GANs intend to minimize. This is because when the data and

generator distributions have non-overlapping supports, which are often the case for high-dimensional data supported by low-dimensional manifolds, the gradient of the JS divergence may provide no useful guidance to optimize the generator [Arjovsky and Bottou, 2017, Arjovsky et al., 2017, Mescheder et al., 2018, Roth et al., 2017]. For this reason, Arjovsky et al. [2017] propose to instead use the Wasserstein-1 distance, which in theory can provide useful gradient for the generator even if the two distributions have disjoint supports. However, Wasserstein GANs often require the use of a critic function under the 1-Lipschitz constraint, which is difficult to satisfy in practice and hence realized with heuristics such as weight clipping Arjovsky et al. [2017], gradient penalty [Gulrajani et al., 2017], and spectral normalization [Miyato et al., 2018].

While the divergence minimization perspective has played an important role in motivating the construction of Wasserstein GANs and gradient penalty-based regularizations, cautions should be made on purely relying on this perspective to understand GAN training, due to not only the discrepancy between the divergence in theory and the actual min-max objective function used in practice, but also the potential confounding between different divergences and different training and regularization strategies [Fedus et al., 2018, Mescheder et al., 2018]. For example, Mescheder et al. [2018] have provided a simple example where in theory the Wasserstein GAN is predicted to succeed while the vanilla GAN is predicted to fail, but in practice the Wasserstein GAN with a finite number of discriminator updates per generator update fails to converge while the vanilla GAN that trains its generator with the non-saturating loss can slowly converge. Fedus et al. [2018] provide a rich set of empirical evidence to discourage viewing GANs purely from the perspective of minimizing a specific divergence at each training step and emphasize the important role played by gradient penalties on stabilizing GAN training.

Diffusion models. Due to the use of a forward diffusion chain, the proposed Diffusion-GAN can be related to diffusion-based (or score-based) deep generative models [Ho et al., 2020, Sohl-Dickstein et al., 2015, Song and Ermon, 2019] that employ both a forward (inference) and a reverse (generative) diffusion chain. These diffusion-based generative models are stable to train and can generate high-fidelity photo-realistic images [Dhariwal and Nichol, 2021, Ho et al., 2020, Nichol et al., 2021, Ramesh et al., 2022, Song and Ermon, 2019, Song et al., 2021b]. However, they are notoriously slow in generation due to the need to traverse the reverse diffusion chain, which involves going through the same U-Net-based generator network hundreds or even thousands of times [Song et al., 2021a]. For this reason, a variety of methods have been recently proposed to reduce the generation cost of diffusion-based generative models [Kong and Ping, 2021, Luhman and Luhman, 2021, Pandey et al., 2022, San-Roman et al., 2021, Song et al., 2021a, Xiao et al., 2021, Zheng et al., 2022]. From the optimization perspective, the loss function of a denoising diffusion model, defined with (2) and (4), involves the summation of $\mathcal{D}_{\text{KL}}(q(x_{t-1} | x_t) || p_{\theta}(x_{t-1} | x_t))$ over different t , which is reformulated into the summation of $\mathcal{D}_{\text{KL}}(q(x_{t-1} | x_t, x_0) || p_{\theta}(x_{t-1} | x_t))$ for tractable estimation [Ho et al., 2020, Sohl-Dickstein et al., 2015].

Different from denoising diffusion, as shown in (8) and (9), the proposed Diffusion-GAN is minimizing the summation of the JS divergence between the diffused real data distribution and diffused generator distribution over different t . Thus a key distinction is that Diffusion-GAN needs a reverse diffusion chain during neither training nor generation. More specifically, its generator, which is updated during training by backpropagating the gradient first through the forward diffusion chain and then through the discriminator, maps the noise to a generated sample in a single step during generation. Therefore, Diffusion-GAN can train and generate almost as quickly as a vanilla GAN does with the same network size.

Differentiable augmentation. As Diffusion-GAN transforms both the data and generated samples before sending them to the discriminator, we can also relate it to differentiable augmentation [Karras et al., 2020a, Zhao et al., 2020] proposed for data-efficient GAN training. Karras et al. [2020a] introduce a stochastic augmentation pipeline with 18 transformations and develop an adaptive mechanism for controlling the augmentation probability. Zhao et al.

[2020] propose to use *Color + Translation + Cutout* as differentiable augmentations for both generated and real images.

While providing good empirical results on some datasets, these augmentation methods are developed with domain-specific knowledge and have the risk of leaking augmentation into generation [Karras et al., 2020a]. As observed in our experiments, they sometime worsen the results when applied to a new dataset, likely because the risk of augmentation leakage overpowers the benefits of enlarging the training set, which could happen especially if the training set size is already sufficiently large.

By contrast, Diffusion-GAN uses a differentiable forward diffusion process to stochastically transform the data and can be considered as both a domain-agnostic and a model-agnostic augmentation method. In other words, Diffusion-GAN can be applied to non-image data or even latent features, for which appropriate data augmentation is difficult to be defined, and easily plugged into an existing GAN to improve its generation performance. Moreover, we prove in theory and show in experiments that augmentation leakage is not a concern for Diffusion-GAN. Tran et al. [2021] provide a theoretical analysis for deterministic non-leaking transformation with differentiable and invertible mapping functions. Bora et al. [2018] show similar theorems to us for specific stochastic transformations, such as Gaussian Projection, Convolve+Noise, and stochastic Block-Pixels, while our Theorem 2 includes more satisfying possibilities as discussed in Appendix A.

4 Experiments

We conduct extensive experiments to answer the following questions: **(a)** What does Theorem 1 reflect in empirical training? **(b)** Will the diffusion-based noise injection help the learning of GANs in domain-agnostic tasks? **(c)** Whether Diffusion-GANs have better mode coverage? **(d)** Will our method improve the performance of GANs trained with limited data? **(e)** How does our method prevent discriminator overfitting? **(f)** Will Diffusion-GAN outperform state-of-the-art baselines on benchmark datasets? We will show four sets of experiments to answer the aforementioned questions. First, we experiment on a toy example with an analytic JS divergence to answer question **(a)**. Then, we show domain-agnostic experiments to mainly address questions **(b)** and **(c)**. The limited data experiments answer question **(d)**. The final set of experiments address questions **(e)** and **(f)**.

Datasets. We conduct experiments on image datasets ranging from low-resolution (*e.g.*, 32×32) to high-resolution (*e.g.*, 1024×1024) and from low-diversity to high-diversity: CIFAR-10 [Krizhevsky, 2009], STL-10 [Coates et al., 2011], LSUN-Bedroom [Yu et al., 2015], LSUN-Church [Yu et al., 2015], AFHQ(Cat/Dog/Wild) [Choi et al., 2020], and FFHQ [Karras et al., 2019]. More details on these benchmark datasets are provided in Appendix E.

Evaluation protocol. We measure image quality using FID [Heusel et al., 2017]. Following Karras et al. [2019, 2020b], we measure FID using 50k generated samples, with the full training set used as reference. We use the number of real images shown to the discriminator to evaluate convergence [Karras et al., 2020a, Sauer et al., 2021]. Unless specified otherwise, all models are trained with 50 million images to ensure convergence (these trained with more or fewer images are specified in table captions). We further report the improved *Recall* score introduced by Kynkäänniemi et al. [2019] to measure the sample diversity of generative models.

Implementations and baselines. We build Diffusion-GANs based on the code of either StyleGAN2 [Karras et al., 2020b] or ProjectedGAN Sauer et al. [2021]. Diffusion GANs inherit from their corresponding base GANs all their network architectures and training hyperparameters, whose details are provided in Appendix G. Specifically for StyleGAN2, we construct the discriminator as $D_\phi(\mathbf{y}, t)$, where t is injected via its mapping network. For ProjectedGAN, we construct the discriminator as $D_\phi(\mathbf{y})$, where t is ignored to simplify the implementation and minimize the modifications to ProjectedGAN. Plugging the diffusion-based

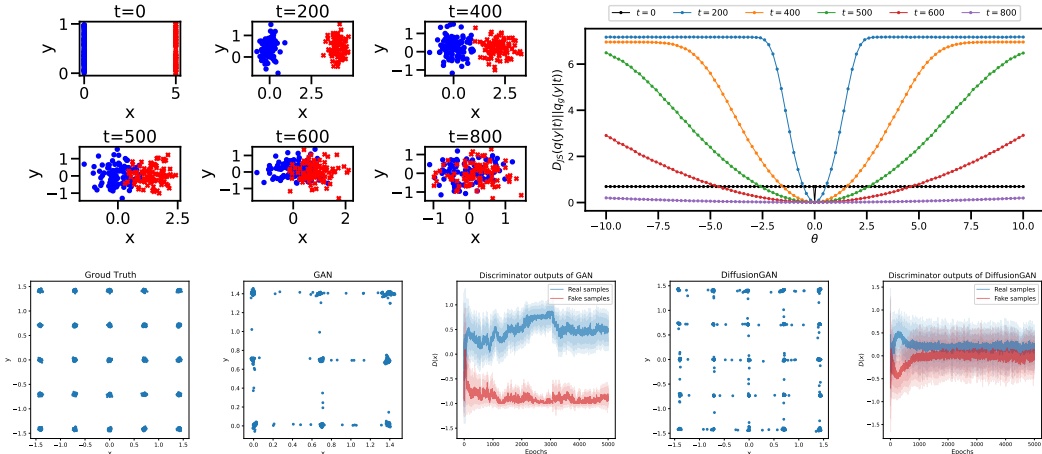


Figure 2: We conduct two toy experiments: (a) the toy example inherited from Arjovsky et al. [2017] and (b) the 25-Gaussians example. For (a), the first row plots the distributions of data with diffusion noise injected for t and the second row shows the JS divergence with and without our noise injection. For (b), the last row shows the true data samples, the generated samples from vanilla GANs, the discriminator outputs of the vanilla GANs, the generated samples from our Diffusion-GAN, and the discriminator outputs of Diffusion-GAN.

noise into the data augmentation pipeline, we denote our models as Diffusion StyleGAN2 and Diffusion ProjectedGAN. To evaluate the effectiveness of the domain-agnostic augmentation method introduced by Diffusion-GANs, we compare it with both StyleGAN2 + DiffAug [Zhao et al., 2020] and StyleGAN2 + ADA [Karras et al., 2020a]. To evaluate whether our domain-agnostic augmentation method could be complementary to existing domain-knowledge-based ones, we further plug it into the augmentation pipeline of StyleGAN2 + DiffAug or ADA. For each benchmark dataset, other state-of-the-art GANs and diffusion models are also included for comparison. In the following experiments, we train related models with their official code if the results are unavailable, while others are all reported from references and marked with *. We run all our experiments with either 4 or 8 NVIDIA V100 GPUs depending on the demands of the inherited training configurations.

Toy example. We consider the same toy example in Arjovsky et al. [2017]. Denote $\mathbf{x} = (0, z)$ as the real data and $\mathbf{x}_g = (\theta, z)$ as the generated data, where $z \sim \text{Unif}(0, 1)$ is a uniform random number and θ is the sole parameter of the generator. In this case, $\mathcal{D}_{\text{JS}}(p(\mathbf{x})||p(\mathbf{x}_g))$ is not continuous: if $\theta = 0$, $\mathcal{D}_{\text{JS}}(p(\mathbf{x})||p(\mathbf{x}_g)) = \log 2$, otherwise $\mathcal{D}_{\text{JS}}(p(\mathbf{x})||p(\mathbf{x}_g)) = 0$, so that it can not provide a usable gradient to drive θ towards 0. With diffusion-based noise injection, as shown in Figure 2 (1st row, left), the supports of \mathbf{y} and \mathbf{y}_g are both the whole metric space \mathbb{R}^2 and their high density regions overlap with each other at different levels depending on t . We show how $\mathcal{D}_{\text{JS}}(q(\mathbf{y}|t)||q_g(\mathbf{y}|t))$ changes as a function of θ under various t values in Figure 2 (1st row, right), where the black line with $t = 0$ shows the original JS divergence, which is not continuous at $\theta = 0$, while as the diffusion step t increases, the JS divergence lines become smoother but provide useful gradients for a wider range of θ . For this reason, a smaller t drives the optimal discriminator to become more assertive while a larger t makes it become more neutral. Thus the diffusion here works like a scale to balance the power of the discriminator. This motivates the use of a differentiable forward diffusion chain that could provide various levels of gradient smoothness to aid the generator training.

4.1 Experiments for domain-agnostic augmentation

To verify whether our method is domain-agnostic, we apply Diffusion-GAN onto the input feature vectors of GANs. We conduct experiments on both low-dimensional and high-dimensional feature vectors, for which commonly used image augmentation methods are not applica-

ble.

25-Gaussians Example. We conduct experiments on the popular 25-Gaussians generation task. The 25-Gaussians dataset is a 2-D toy data, generated by a mixture of 25 two-dimensional Gaussian distributions. Each data point is a 2-dimensional feature vector. We train a small GAN model, whose generator and discriminator are both parameterized by multilayer perceptrons (MLPs), with two 128-unit hidden layers and LeakyReLU nonlinearities.

The training results are shown in Figure 2 (2nd row). We observe that the vanilla GAN exhibits severe mode collapsing, capturing only a few modes. Its discriminator outputs of real and fake samples depart from each other very quickly. This implies a strong overfitting of the discriminator happened so that the discriminator stops providing useful learning signals for the generator. However, Diffusion-GAN successfully captures all the 25 Gaussian modes and the discriminator is under control to continuously provide useful learning signals. We interpret the improvement from two perspectives: first, non-leaking augmentation helps provide more information about the data space; second, the discriminator is well behaved given the adaptively adjusted diffusion-based noise injection.

Projected GAN. To verify that our adaptive diffusion-based noise injection could benefit the learning of GAN on high-dimensional feature vectors, we directly apply it onto the discriminator feature space of ProjectedGAN [Sauer et al., 2021]. ProjectedGANs generally leverage pre-trained neural networks to extract meaningful features for the adversarial learning of the discriminator and generator. Following Sauer et al. [2021], we adaptively diffuse the feature vectors extracted by EfficientNet-v0 and keep all the other training part unchanged. Below we will report the performance of Diffusion ProjectedGAN on several benchmark datasets, which verifies that our augmentation method is domain-agnostic.

4.2 Limited data experiments

In this experiment, we evaluate whether Diffusion-GAN can provide data-efficient GAN training. We first generate four STL-10 (64×64) dataset splits, consisting of 5k, 10k, 50k, and 100k images, respectively (100k denotes the full STL-10). Note that STL-10 is a diverse dataset with 10 different classes so that training STL-10 with a small number of images is considered as a challenging task. We also consider AFHQ-Cat, -Dog, and -Wild, each with as few as around 5k images. We compare Diffusion-GANs with relevant baseline models on these datasets and show the results in Table 1.

Beat backbone models. We first observe that Diffusion-GANs almost always outperform their backbone models, *i.e.*, StyleGAN2 or ProjectedGAN, across various datasets, especially when the dataset size is small. In particular, we find consistent improvement when applying our method onto the high-dimensional feature spaces, where no ambient knowledge is available. Diffusion ProjectedGAN outperforms all the other models by a large margin in all STL splits. This coincides with our theoretical analysis that augmentation leakage is not a concern for Diffusion-GANs.

Comparison to domain-specific augmentations. In limited-data cases, such as the AFHQ datasets and 5k/10k STL splits, our diffusion-based noise injection works as well as Diffaug while underperforms ADA. Note that since our diffusion-based noise injection is totally domain-agnostic, it is not surprising to find out that domain-specific augmentation, developed using prior knowledge on images, is more useful when there is a limited number of images. However, when the dataset becomes large enough such that the risk of leakage overshadows the benefits of domain-knowledge-based augmentation, StleGAN2 + Diffaug/ADA actually makes StyleGAN2 become worse, such as 50k and 100k splits, while our noise injection method almost always improves the backbone model. In other words, our method can improve the performance of GANs on both large and limited datasets.

Complementariness. The complementariness of our method with Diffaug and ADA

Table 1: **AFHQ** FID results and **STL-10** FID results with 5k, 10k, 50k, and 100k training samples. To ensure convergence, all models are trained across 50M images for the 100k split, 25M images for 5k, 10k, and 50k splits, and 25M images for AFHQ datasets respectively. We bold the best number in each column.

Models	AFHQ-Cat (512 × 512, ~5k)	AFHQ-Dog (512 × 512, ~5k)	AFHQ-Wild (512 × 512, ~5k)	STL-10 (64 × 64, 5k)	STL-10 (64 × 64, 10k)	STL-10 (64 × 64, 50k)	STL-10 (64 × 64, 100k)
Diffusion ProjectedGAN	5.62	11.53	5.73	15.00	11.86	10.64	6.91
ProjectedGAN [Sauer et al., 2021]	5.63	11.56	7.40	15.51	14.80	17.50	7.76
Diffusion StyleGAN2	4.09	16.20	3.73	44.33	29.06	15.32	11.43
StyleGAN2 [Karras et al., 2020a]	5.13	19.37	3.48	55.38	40.60	15.35	11.70
StyleGAN2 + Diffaug [Zhao et al., 2020]	6.43	12.79	5.01	42.07	30.03	15.70	12.97
StyleGAN2 + ADA [Karras et al., 2020a]	3.55*	7.40*	3.05*	31.22	22.41	15.83	13.72
Diffusion StyleGAN2 + Diffaug	5.36	8.48	6.24	32.35	23.96	16.55	13.00
Diffusion StyleGAN2 + ADA	3.44	7.49	3.62	31.19	22.54	15.61	14.51

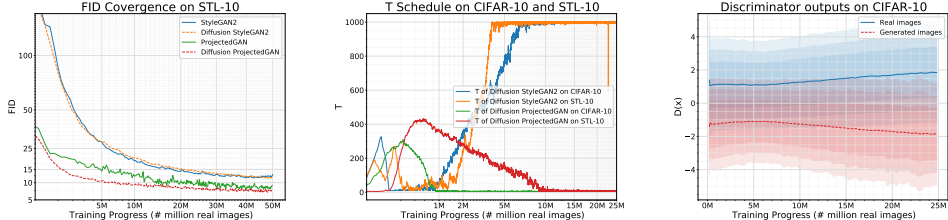


Figure 3: Plots of FID, maximum number of diffusion steps T and discriminator outputs of Diffusion-GANs.

techniques depends on datasets, *e.g.*, Diffusion + Diffaug outperforms Diffaug in 5k and 10k splits, while works slightly worse than Diffaug in the 50k split. This is because the combination of our method with other domain-specific augmentation is possible to leak augmentations in generation. In most cases, we observe that our method is complementary with Diffaug.

4.3 Comparison to state-of-the-arts

We compare Diffusion-GANs with state-of-the-art baselines among diffusion models and GANs in terms of sample fidelity (FID) and sample diversity (Recall) across extensive benchmark datasets.

Before providing detailed comparison, we first illustrate in Figure 3 the convergence of FID, maximum timestep T and discriminator outputs. We see that T is adaptively adjusted: the T for Diffusion StyleGAN2 increases as the training goes while the T for Diffusion ProjectedGAN first goes up and then goes down. Note that the T is adjusted according to the overfitting status of the discriminator. The third panel shows that trained with the diffusion-based mixture distribution, the discriminator is always well-behaved and provides useful learning signals for the generator.

Low resolution tasks. We present the quantitative and qualitative results in Figure 4. Under the StyleGAN2 framework, we observe that Diffusion StyleGAN2 clearly outperforms StyleGAN2 across all datasets, which also empirically validates our Theorem 2. Under the ProjectedGAN framework, we see that with noise properly injected onto the high-dimensional feature space, Diffusion ProjectedGAN shows big and consistent improvement in terms of both FID and Recall. We reach state-of-the-art FID results with Diffusion ProjectedGAN on STL-10 and LSUN-Bedroom/Church datasets.

From the data augmentation perspective, Diffusion StyleGAN2 outperforms Diffaug and ADA on 3 out of 4 datasets while slightly underperforms ADA only on CIFAR-10 in terms of FID. Diffusion StyleGAN2 also provides better sample diversity, especially for CIFAR-10, reflected by the Recall results. Echoing the observations in Table 1, we notice that ADA and Diffaug could sometimes impair the generation performance when the dataset size is already sufficiently large, *i.e.*, LSUN-Bedroom and LSUN-Church, while this is not a concern for Diffusion-GAN. From the diffusion model perspective, Diffusion-GAN outperforms representative diffusion-

Low Resolution Tasks	CIFAR-10 (32 × 32)		STL-10 (64 × 64)		LSUN-Bedroom (256 × 256)		LSUN-Church (256 × 256)	
	FID	Recall	FID	Recall	FID	Recall	FID	Recall
DDPM [Ho et al., 2020]*	3.21	0.57	-	-	4.90	-	7.89	-
DDIM [Song et al., 2021a]*	4.67	0.53	-	-	6.62	-	10.58	-
Denoising Diffusion-GAN [Xiao et al., 2021]*	3.75	0.57	-	-	-	-	5.25	-
Styleformer [Park and Kim, 2021]	2.82*	-	26.10	-	-	-	-	-
PG-GAN [Karras et al., 2018]*	-	-	-	-	8.34	-	6.42	-
PNDM [Liu et al., 2022]*	3.60	-	-	-	5.68	-	8.69	-
ADM [Dhariwal and Nichol, 2021]*	-	-	-	-	1.90	-	-	-
CIPS [Anokhin et al., 2021]*	-	-	-	-	-	-	2.92	-
StyleGAN2 [Karras et al., 2020a]	8.32*	0.41*	11.70	0.44	3.98	0.32	3.93	0.39
StyleGAN2 + Diffaug [Zhao et al., 2020]	5.79*	0.42*	12.97	0.39	4.25	0.19	4.66	0.33
StyleGAN2 + ADA [Karras et al., 2020a]	2.92*	0.49*	13.72	0.36	7.89	0.05	4.12	0.18
Diffusion StyleGAN2	3.19	0.58	11.53	0.45	3.65	0.32	3.17	0.41
Diffusion StyleGAN2 + Diffaug	2.92	0.58	13.00	0.39	5.07	0.13	4.88	0.29
Diffusion StyleGAN2 + ADA	2.67	0.59	14.51	0.31	4.33	0.25	3.38	0.37
ProjectedGAN [Sauer et al., 2021]	3.10	0.45	7.76	0.35	2.25	0.55	3.42	0.56
Diffusion ProjectedGAN	2.54	0.45	6.91	0.35	1.43	0.58	1.85	0.65



(a) Low resolution tasks.

(b) (c) (d) (e)

Figure 4: Unconditional image generation results on low resolution datasets. Styleformer reports FID 15.17 for STL-10 (48×48) while we rerun it on STL-10 (64×64) with its 64 resolution configuration and get 26.10. To ensure convergence, our models and baselines are trained across 100M images for CIFAR-10. We bold the best results under the StyleGAN2 and ProjectedGAN codebases, respectively.

High Resolution Tasks	AFHQ-All (512 × 512)		FFHQ (1024 × 1024)	
	FID	Recall	FID	Recall
StyleGAN2 [Karras et al., 2020a]	6.61	0.25	4.25	0.42
StyleGAN2 + Diffaug [Zhao et al., 2020]	10.59	0.12	4.46	0.41
StyleGAN2 + ADA [Karras et al., 2020a]	5.40	0.32	4.47	0.41
Diffusion StyleGAN2	5.86	0.30	3.71	0.43
Diffusion StyleGAN2 + Diffaug	6.63	0.26	3.89	0.41
Diffusion StyleGAN2 + ADA	4.93	0.34	4.37	0.41



(a) High resolution tasks.

(b) Generated images for AFHQ-All and FFHQ.

Figure 5: Unconditional image generation results on high resolution datasets. To ensure convergence, our models and baselines are trained across 25M images for AFHQ-All and 25M images for FFHQ respectively. Karras et al. [2020a] report FID 5.28 for StyleGAN2 and 4.30 for StyleGAN2+ADA on FFHQ (256×256 , 70k).

based generative models, such as DDPM and PNDM, in terms of both FID and Recall and can generate as quickly as a vanilla GAN by mapping a noise to a data in a single step. Last but not least, we again observe that Diffusion-GAN is complementary to Diffaug and ADA in some cases, however, such complementariness is data dependent and not guaranteed to exist.

High resolution tasks. We conduct experiments to show whether our method is compatible with high resolution tasks. We focus on the StyleGAN2 codebase that is known for its ability to synthesize high-resolution images and report the results in Figure 5. First, we could see that Diffusion StylgeGAN2 clearly outperforms its backbone model. For AFHQ-All, the combination of Diffusion and ADA works the best, while for FFHQ Diffusion StylgeGAN2 works the best. The generated images on the right are all photo-realistic. More randomly generated uncurated images are provided in Appendix H.

5 Conclusion

This paper introduces Diffusion-GAN that employs a Gaussian mixture distribution, defined over all the diffusion steps of a variable-length forward diffusion chain, to inject instance noise into GAN training. The proposed Diffusion-GAN provides differentiable augmentation that is both model- and domain-agnostic, and enjoys the benefits of a diffusion process but does not need to learn a computationally expensive reverse diffusion chain. Theoretically, we show Diffusion-GAN can resist discriminator overfitting and introduce non-leaking augmentation.

Empirically, we conduct extensive experiments on typical benchmark datasets and achieve state-of-the-art results in synthesizing high-resolution photo-realistic images, as measured by both FID for fidelity and Recall for diversity.

References

- Ivan Anokhin, Kirill V. Demochkin, Taras Khakhulin, Gleb Sterkin, Victor S. Lempitsky, and Denis Korzhenkov. Image generators with conditionally-independent pixel synthesis. *2021 IEEE/CVF Conference on Computer Vision and Pattern Recognition (CVPR)*, pages 14273–14282, 2021.
- Martín Arjovsky and Léon Bottou. Towards principled methods for training generative adversarial networks. In *5th International Conference on Learning Representations, ICLR 2017, Toulon, France, April 24-26, 2017, Conference Track Proceedings*. OpenReview.net, 2017. URL https://openreview.net/forum?id=Hk4_qw5xe.
- Martin Arjovsky, Soumith Chintala, and Léon Bottou. Wasserstein generative adversarial networks. In *Proceedings of the 34th International Conference on Machine Learning-Volume 70*, pages 214–223, 2017.
- Marc G Bellemare, Ivo Danihelka, Will Dabney, Shakir Mohamed, Balaji Lakshminarayanan, Stephan Hoyer, and Rémi Munos. The Cramer distance as a solution to biased Wasserstein gradients. *arXiv preprint arXiv:1705.10743*, 2017.
- David M Blei, Alp Kucukelbir, and Jon D McAuliffe. Variational inference: A review for statisticians. *Journal of the American statistical Association*, 112(518):859–877, 2017.
- Ashish Bora, Eric Price, and Alexandros G. Dimakis. AmbientGAN: Generative models from lossy measurements. In *International Conference on Learning Representations*, 2018. URL <https://openreview.net/forum?id=Hy7fDog0b>.
- Andrew Brock, Jeff Donahue, and Karen Simonyan. Large scale GAN training for high fidelity natural image synthesis. *arXiv preprint arXiv:1809.11096*, 2018.
- Yunjey Choi, Youngjung Uh, Jaejun Yoo, and Jung-Woo Ha. StarGAN v2: Diverse image synthesis for multiple domains. *2020 IEEE/CVF Conference on Computer Vision and Pattern Recognition (CVPR)*, pages 8185–8194, 2020.
- Adam Coates, Andrew Ng, and Honglak Lee. An analysis of single-layer networks in unsupervised feature learning. In *Proceedings of the fourteenth international conference on artificial intelligence and statistics*, pages 215–223. JMLR Workshop and Conference Proceedings, 2011.
- Jia Deng, Wei Dong, Richard Socher, Li-Jia Li, Kai Li, and Li Fei-Fei. Imagenet: A large-scale hierarchical image database. In *2009 IEEE conference on computer vision and pattern recognition*, pages 248–255. Ieee, 2009.
- Ishan Deshpande, Ziyu Zhang, and Alexander G Schwing. Generative modeling using the sliced Wasserstein distance. In *Proceedings of the IEEE conference on computer vision and pattern recognition*, pages 3483–3491, 2018.
- Prafulla Dhariwal and Alexander Quinn Nichol. Diffusion models beat GANs on image synthesis. In A. Beygelzimer, Y. Dauphin, P. Liang, and J. Wortman Vaughan, editors, *Advances in Neural Information Processing Systems*, 2021. URL <https://openreview.net/forum?id=AAWuCvzaVt>.
- Jeff Donahue, Philipp Krähenbühl, and Trevor Darrell. Adversarial feature learning. *arXiv preprint arXiv:1605.09782*, 2016.

- Vincent Dumoulin, Ishmael Belghazi, Ben Poole, Olivier Mastropietro, Alex Lamb, Martin Arjovsky, and Aaron Courville. Adversarially learned inference. *arXiv preprint arXiv:1606.00704*, 2016.
- William Fedus, Mihaela Rosca, Balaji Lakshminarayanan, Andrew M Dai, Shakir Mohamed, and Ian Goodfellow. Many paths to equilibrium: GANs do not need to decrease a divergence at every step. In *International Conference on Learning Representations*, 2018.
- Ian Goodfellow, Jean Pouget-Abadie, Mehdi Mirza, Bing Xu, David Warde-Farley, Sherjil Ozair, Aaron Courville, and Yoshua Bengio. Generative adversarial nets. In *Advances in Neural Information Processing Systems*, pages 2672–2680, 2014.
- Ishaan Gulrajani, Faruk Ahmed, Martin Arjovsky, Vincent Dumoulin, and Aaron C Courville. Improved training of Wasserstein GANs. In *Advances in Neural Information Processing Systems*, pages 5767–5777, 2017.
- Martin Heusel, Hubert Ramsauer, Thomas Unterthiner, Bernhard Nessler, and Sepp Hochreiter. GANs trained by a two time-scale update rule converge to a local Nash equilibrium. In *Advances in Neural Information Processing Systems*, pages 6626–6637, 2017.
- Jonathan Ho, Ajay Jain, and Pieter Abbeel. Denoising diffusion probabilistic models. *Advances in Neural Information Processing Systems*, 33:6840–6851, 2020.
- Michael I Jordan, Zoubin Ghahramani, Tommi S Jaakkola, and Lawrence K Saul. An introduction to variational methods for graphical models. *Machine learning*, 37(2):183–233, 1999.
- Tero Karras, Timo Aila, Samuli Laine, and Jaakko Lehtinen. Progressive growing of GANs for improved quality, stability, and variation. In *International Conference on Learning Representations*, 2018.
- Tero Karras, Samuli Laine, and Timo Aila. A style-based generator architecture for generative adversarial networks. In *Proceedings of the IEEE/CVF Conference on Computer Vision and Pattern Recognition*, pages 4401–4410, 2019.
- Tero Karras, Miika Aittala, Janne Hellsten, Samuli Laine, Jaakko Lehtinen, and Timo Aila. Training generative adversarial networks with limited data. *Advances in Neural Information Processing Systems*, 33:12104–12114, 2020a.
- Tero Karras, Samuli Laine, Miika Aittala, Janne Hellsten, Jaakko Lehtinen, and Timo Aila. Analyzing and improving the image quality of stylegan. In *Proceedings of the IEEE/CVF conference on computer vision and pattern recognition*, pages 8110–8119, 2020b.
- Diederik P. Kingma and Max Welling. Auto-encoding variational Bayes. *CoRR*, abs/1312.6114, 2014.
- Zhifeng Kong and Wei Ping. On fast sampling of diffusion probabilistic models. *arXiv preprint arXiv:2106.00132*, 2021.
- Alex Krizhevsky. Learning multiple layers of features from tiny images. 2009.
- Tuomas Kynkäänniemi, Tero Karras, Samuli Laine, Jaakko Lehtinen, and Timo Aila. Improved precision and recall metric for assessing generative models. *Advances in Neural Information Processing Systems*, 32, 2019.
- Chun-Liang Li, Wei-Cheng Chang, Yu Cheng, Yiming Yang, and Barnabás Póczos. MMD GAN: Towards deeper understanding of moment matching network. *Advances in neural information processing systems*, 30, 2017a.

- Chunyuan Li, Hao Liu, Changyou Chen, Yuchen Pu, Liqun Chen, Ricardo Henao, and Lawrence Carin. Alice: Towards understanding adversarial learning for joint distribution matching. *Advances in neural information processing systems*, 30, 2017b.
- Luping Liu, Yi Ren, Zhijie Lin, and Zhou Zhao. Pseudo numerical methods for diffusion models on manifolds. *ArXiv*, abs/2202.09778, 2022.
- Eric Luhman and Troy Luhman. Knowledge distillation in iterative generative models for improved sampling speed. *arXiv preprint arXiv:2101.02388*, 2021.
- Lars Mescheder, Sebastian Nowozin, and Andreas Geiger. The numerics of GANs. *Advances in neural information processing systems*, 30, 2017.
- Lars Mescheder, Andreas Geiger, and Sebastian Nowozin. Which training methods for GANs do actually converge? In *International conference on machine learning*, pages 3481–3490. PMLR, 2018.
- Takeru Miyato, Toshiki Kataoka, Masanori Koyama, and Yuichi Yoshida. Spectral normalization for generative adversarial networks. In *International Conference on Learning Representations*, 2018. URL <https://openreview.net/forum?id=B1QRgziT->.
- Alex Nichol, Prafulla Dhariwal, Aditya Ramesh, Pranav Shyam, Pamela Mishkin, Bob McGrew, Ilya Sutskever, and Mark Chen. Glide: Towards photorealistic image generation and editing with text-guided diffusion models. *arXiv preprint arXiv:2112.10741*, 2021.
- Sebastian Nowozin, Botond Cseke, and Ryota Tomioka. f-gan: Training generative neural samplers using variational divergence minimization. In *Advances in neural information processing systems*, 2016.
- Kushagra Pandey, Avideep Mukherjee, Piyush Rai, and Abhishek Kumar. Diffusevae: Efficient, controllable and high-fidelity generation from low-dimensional latents. *arXiv preprint arXiv:2201.00308*, 2022.
- Jeeseung Park and Youngeun Kim. Styleformer: Transformer based generative adversarial networks with style vector. *ArXiv*, abs/2106.07023, 2021.
- Alec Radford, Luke Metz, and Soumith Chintala. Unsupervised representation learning with deep convolutional generative adversarial networks. *CoRR*, abs/1511.06434, 2016.
- Aditya Ramesh, Prafulla Dhariwal, Alex Nichol, Casey Chu, and Mark Chen. Hierarchical text-conditional image generation with CLIP latents. *arXiv preprint arXiv:2204.06125*, 2022.
- Kevin Roth, Aurelien Lucchi, Sebastian Nowozin, and Thomas Hofmann. Stabilizing training of generative adversarial networks through regularization. *Advances in neural information processing systems*, 30, 2017.
- Tim Salimans, Ian Goodfellow, Wojciech Zaremba, Vicki Cheung, Alec Radford, and Xi Chen. Improved techniques for training GANs. In *Advances in Neural Information Processing Systems*, pages 2234–2242, 2016.
- Robin San-Roman, Eliya Nachmani, and Lior Wolf. Noise estimation for generative diffusion models. *arXiv preprint arXiv:2104.02600*, 2021.
- Axel Sauer, Kashyap Chitta, Jens Müller, and Andreas Geiger. Projected gans converge faster. *Advances in Neural Information Processing Systems*, 34, 2021.
- Jascha Sohl-Dickstein, Eric A. Weiss, Niru Maheswaranathan, and Surya Ganguli. Deep unsupervised learning using nonequilibrium thermodynamics. *ArXiv*, abs/1503.03585, 2015.

- Casper Kaae Sønderby, Jose Caballero, Lucas Theis, Wenzhe Shi, and Ferenc Huszár. Amortised MAP inference for image super-resolution. In *5th International Conference on Learning Representations, ICLR 2017, Toulon, France, April 24-26, 2017, Conference Track Proceedings*. OpenReview.net, 2017. URL <https://openreview.net/forum?id=S1RP6GL1e>.
- Jiaming Song, Chenlin Meng, and Stefano Ermon. Denoising diffusion implicit models. In *International Conference on Learning Representations*, 2021a. URL <https://openreview.net/forum?id=St1giarCHLP>.
- Yang Song and Stefano Ermon. Generative modeling by estimating gradients of the data distribution. In *Advances in Neural Information Processing Systems*, pages 11918–11930, 2019.
- Yang Song, Jascha Sohl-Dickstein, Diederik P Kingma, Abhishek Kumar, Stefano Ermon, and Ben Poole. Score-based generative modeling through stochastic differential equations. In *International Conference on Learning Representations*, 2021b. URL <https://openreview.net/forum?id=PxtIG12RRHS>.
- Ngoc-Trung Tran, Viet-Hung Tran, Ngoc-Bao Nguyen, Trung-Kien Nguyen, and Ngai-Man Cheung. On data augmentation for gan training. *IEEE Transactions on Image Processing*, 30:1882–1897, 2021.
- Ting-Chun Wang, Ming-Yu Liu, Jun-Yan Zhu, Andrew Tao, Jan Kautz, and Bryan Catanzaro. High-resolution image synthesis and semantic manipulation with conditional GANs. In *Proceedings of the IEEE conference on computer vision and pattern recognition*, pages 8798–8807, 2018.
- Zhisheng Xiao, Karsten Kreis, and Arash Vahdat. Tackling the generative learning trilemma with denoising diffusion gans. *ArXiv*, abs/2112.07804, 2021.
- Fisher Yu, Ari Seff, Yinda Zhang, Shuran Song, Thomas Funkhouser, and Jianxiong Xiao. Lsun: Construction of a large-scale image dataset using deep learning with humans in the loop. *arXiv preprint arXiv:1506.03365*, 2015.
- Han Zhang, Tao Xu, Hongsheng Li, Shaoting Zhang, Xiaogang Wang, Xiaolei Huang, and Dimitris N Metaxas. StackGAN: Text to photo-realistic image synthesis with stacked generative adversarial networks. In *Proceedings of the IEEE international conference on computer vision*, pages 5907–5915, 2017.
- Han Zhang, Ian Goodfellow, Dimitris Metaxas, and Augustus Odena. Self-attention generative adversarial networks. In *International Conference on Machine Learning*, pages 7354–7363. PMLR, 2019.
- Han Zhang, Zizhao Zhang, Augustus Odena, and Honglak Lee. Consistency regularization for generative adversarial networks. In *International Conference on Learning Representations*, 2020a. URL <https://openreview.net/forum?id=S1lxK1SKPH>.
- Hao Zhang, Bo Chen, Long Tian, Zhengjue Wang, and Mingyuan Zhou. Variational hetero-encoder randomized GANs for joint image-text modeling. In *International Conference on Learning Representations*, 2020b. URL <https://openreview.net/forum?id=H1x5wRVtvS>.
- Shengyu Zhao, Zhijian Liu, Ji Lin, Jun-Yan Zhu, and Song Han. Differentiable augmentation for data-efficient gan training. *Advances in Neural Information Processing Systems*, 33: 7559–7570, 2020.
- Huangjie Zheng and Mingyuan Zhou. Exploiting chain rule and Bayes’ theorem to compare probability distributions. In A. Beygelzimer, Y. Dauphin, P. Liang, and J. Wortman Vaughan, editors, *Advances in Neural Information Processing Systems*, 2021. URL <https://openreview.net/forum?id=f-ggKIDTu5D>.

Huangjie Zheng, Pengcheng He, Weizhu Chen, and Mingyuan Zhou. Truncated diffusion probabilistic models. *arXiv preprint arXiv:2202.09671*, 2022.

Appendix

A Proof

Proof of Theorem 1. For simplicity, let $\mathbf{x} \sim \mathbb{P}_r$, $\mathbf{x}_g \sim \mathbb{P}_g$, $\mathbf{y} \sim \mathbb{P}_{r',t}$, $\mathbf{y}_g \sim \mathbb{P}_{g',t}$, $a_t = \sqrt{\bar{\alpha}_t}$ and $b_t = (1 - \bar{\alpha}_t)\sigma^2$. Then,

$$\begin{aligned} p_{r',t}(\mathbf{y}) &= \int_{\mathcal{X}} p_r(\mathbf{x}) \mathcal{N}(\mathbf{y}; a_t \mathbf{x}, b_t \mathbf{I}) d\mathbf{x} \\ p_{g',t}(\mathbf{y}) &= \int_{\mathcal{X}} p_g(\mathbf{x}) \mathcal{N}(\mathbf{y}; a_t \mathbf{x}, b_t \mathbf{I}) d\mathbf{x} \\ \mathbf{z} &\sim p(\mathbf{z}), \mathbf{x}_g = g_\theta(\mathbf{z}), \mathbf{y}_g = a_t \mathbf{x}_g + b_t \boldsymbol{\epsilon}, \boldsymbol{\epsilon} \sim p(\boldsymbol{\epsilon}) \end{aligned}$$

$$\begin{aligned} \mathcal{D}_f(p_{r',t}(\mathbf{y}) || p_{g',t}(\mathbf{y})) &= \int_{\mathcal{X}} p_{g',t}(\mathbf{y}) f\left(\frac{p_{r',t}(\mathbf{y})}{p_{g',t}(\mathbf{y})}\right) d\mathbf{y} \\ &= \mathbb{E}_{\mathbf{y} \sim p_{g',t}(\mathbf{y})} \left[f\left(\frac{p_{r',t}(\mathbf{y})}{p_{g',t}(\mathbf{y})}\right) \right] \\ &= \mathbb{E}_{\mathbf{z} \sim p(\mathbf{z}), \boldsymbol{\epsilon} \sim p(\boldsymbol{\epsilon})} \left[f\left(\frac{p_{r',t}(a_t g_\theta(\mathbf{z}) + b_t \boldsymbol{\epsilon})}{p_{g',t}(a_t g_\theta(\mathbf{z}) + b_t \boldsymbol{\epsilon})}\right) \right] \end{aligned}$$

Since $\mathcal{N}(\mathbf{y}; a_t \mathbf{x}, b_t \mathbf{I})$ is assumed to be an isotropic Gaussian distribution, for simplicity, in what follows we show the proof in uni-variate Gaussian, which could be easily extended to multi-variate Gaussian by the production rule. We first show that under mild conditions, the $p_{r',t}(y)$ and $p_{g',t}(y)$ are continuous functions over y .

$$\begin{aligned} \lim_{\Delta y \rightarrow 0} p_{r',t}(y - \Delta y) &= \lim_{\Delta y \rightarrow 0} \int_{\mathcal{X}} p_r(x) \mathcal{N}(y - \Delta y; a_t x, b_t) dx \\ &= \int_{\mathcal{X}} p_r(x) \lim_{\Delta y \rightarrow 0} \mathcal{N}(y - \Delta y; a_t x, b_t) dx \\ &= \int_{\mathcal{X}} p_r(x) \lim_{\Delta y \rightarrow 0} \frac{1}{C_1} \exp\left(\frac{((y - \Delta y) - a_t x)^2}{C_2}\right) dx \\ &= \int_{\mathcal{X}} p_r(x) \mathcal{N}(y; a_t x, b_t) dx \\ &= p_{r',t}(y), \end{aligned}$$

where C_1 and C_2 are constants. Hence, $p_{r',t}(y)$ is a continuous function defined on y . The proof of continuity for $p_{g',t}(y)$ is exactly the same proof. Then, given g_θ is also a continuous function, it is clear to see that $\mathcal{D}_f(p_{r',t}(\mathbf{y}) || p_{g',t}(\mathbf{y}))$ is a continuous function over θ .

Next, we show that $\mathcal{D}_f(p_{r',t}(\mathbf{y}) || p_{g',t}(\mathbf{y}))$ is differentiable. By the chain rule, showing $\mathcal{D}_f(p_{r',t}(\mathbf{y}) || p_{g',t}(\mathbf{y}))$ to be differentiable is equivalent to show $p_{r',t}(y)$, $p_{g',t}(y)$ and f are differentiable. Usually, f is defined with differentiability [Nowozin et al., 2016].

$$\begin{aligned} \nabla_\theta p_{r',t}(a_t g_\theta(z) + b_t \boldsymbol{\epsilon}) &= \nabla_\theta \int_{\mathcal{X}} p_r(x) \mathcal{N}(a_t g_\theta(z) + b_t \boldsymbol{\epsilon}; a_t x, b_t) dx \\ &= \int_{\mathcal{X}} p_r(x) \frac{1}{C_1} \nabla_\theta \exp\left(\frac{\|a_t g_\theta(z) + b_t \boldsymbol{\epsilon} - a_t x\|_2^2}{C_2}\right) dx, \end{aligned}$$

$$\begin{aligned} \nabla_\theta p_{g',t}(a_t g_\theta(z) + b_t \boldsymbol{\epsilon}) &= \nabla_\theta \int_{\mathcal{X}} p_g(x) \mathcal{N}(a_t g_\theta(z) + b_t \boldsymbol{\epsilon}; a_t x, b_t) dx \\ &= \nabla_\theta \mathbb{E}_{z' \sim p(z')} [\mathcal{N}(a_t g_\theta(z) + b_t \boldsymbol{\epsilon}; a_t g_\theta(z'), b_t)] \\ &= \mathbb{E}_{z' \sim p(z')} \left[\frac{1}{C_1} \nabla_\theta \exp\left(\frac{\|a_t g_\theta(z) + b_t \boldsymbol{\epsilon} - a_t g_\theta(z')\|_2^2}{C_2}\right) \right], \end{aligned}$$

where C_1 and C_2 are constants. Hence, $p_{r',t}(y)$ and $p_{r',t}(y)$ are differentiable, which concludes the proof. \square

Proof of Theorem 2. We have $p(\mathbf{y}) = \int p(\mathbf{x})q(\mathbf{y}|\mathbf{x})d\mathbf{x}$ and $p_g(\mathbf{y}) = \int p_g(\mathbf{x})q(\mathbf{y}|\mathbf{x})d\mathbf{x}$.
 \Leftarrow If $p(\mathbf{x}) = p_g(\mathbf{x})$, then $p(\mathbf{y}) = p_g(\mathbf{y})$
 \Rightarrow Let $\mathbf{y} \sim p(\mathbf{y})$ and $\mathbf{y}_g \sim p_g(\mathbf{y})$. Given the assumption on $q(\mathbf{y}|\mathbf{x})$, we have

$$\begin{aligned}\mathbf{y} &= f(\mathbf{x}) + g(\boldsymbol{\epsilon}), \mathbf{x} \sim p(\mathbf{x}), \boldsymbol{\epsilon} \sim p(\boldsymbol{\epsilon}) \\ \mathbf{y}_g &= f(\mathbf{x}_g) + g(\boldsymbol{\epsilon}_g), \mathbf{x}_g \sim p_g(\mathbf{x}), \boldsymbol{\epsilon}_g \sim p(\boldsymbol{\epsilon}).\end{aligned}$$

Since f and g are one-to-one mapping functions, $f(\mathbf{x})$ and $g(\boldsymbol{\epsilon})$ are identifiable, which indicates $f(\mathbf{x}) \stackrel{D}{=} f(\mathbf{x}_g) \Rightarrow \mathbf{x} \stackrel{D}{=} \mathbf{x}_g$. By the property of moment-generating functions (MGF), given $f(\mathbf{x})$ is independent with $g(\boldsymbol{\epsilon})$, we have for $\forall \mathbf{s}$

$$\begin{aligned}M_{\mathbf{y}}(\mathbf{s}) &= M_{f(\mathbf{x})}(\mathbf{s}) \cdot M_{g(\boldsymbol{\epsilon})}(\mathbf{s}) \\ M_{\mathbf{y}_g}(\mathbf{s}) &= M_{f(\mathbf{x}_g)}(\mathbf{s}) \cdot M_{g(\boldsymbol{\epsilon}_g)}(\mathbf{s}).\end{aligned}$$

where $M_{\mathbf{y}}(\mathbf{s}) = E_{\mathbf{y} \sim p(\mathbf{y})}[e^{\mathbf{s}^T \mathbf{y}}]$ denotes the MGF of random variable \mathbf{y} and the others follow the same form. By the moment-generating function uniqueness theorem, given $\mathbf{y} \stackrel{D}{=} \mathbf{y}_g$ and $g(\boldsymbol{\epsilon}) \stackrel{D}{=} g(\boldsymbol{\epsilon}_g)$, we have $M_{\mathbf{y}}(\mathbf{s}) = M_{\mathbf{y}_g}(\mathbf{s})$ and $M_{g(\boldsymbol{\epsilon})}(\mathbf{s}) = M_{g(\boldsymbol{\epsilon}_g)}(\mathbf{s})$ for $\forall \mathbf{s}$. Then, we could obtain $M_{f(\mathbf{x})} = M_{f(\mathbf{x}_g)}$ for $\forall \mathbf{s}$. Thus, $M_{f(\mathbf{x})} = M_{f(\mathbf{x}_g)} \Rightarrow f(\mathbf{x}) \stackrel{D}{=} f(\mathbf{x}_g) \Rightarrow p(\mathbf{x}) = p(\mathbf{x}_g)$, which concludes the proof.

Discussion. Next, we discuss which $q(\mathbf{y}|\mathbf{x})$ fits the assumption we made on it. We follow the discussion of reparameterization of distributions as used in Kingma and Welling [2014]. Three basic approaches are:

1. Tractable inverse CDF. In this case, let $\boldsymbol{\epsilon} \sim \mathcal{U}(\mathbf{0}, \mathbf{I})$, and $\psi(\boldsymbol{\epsilon}, \mathbf{y}, \mathbf{x})$ be the inverse CDF of $q(\mathbf{y}|\mathbf{x})$. From $\psi(\boldsymbol{\epsilon}, \mathbf{y}, \mathbf{x})$, if $\mathbf{y} = f(\mathbf{x}) + g(\boldsymbol{\epsilon})$, for example, $y \sim \text{Cauchy}(x, \gamma)$ and $y \sim \text{Logistic}(x, s)$, then Theorem 2 holds.
2. Analogous to the Gaussian example, $\mathbf{y} \sim \mathcal{N}(\mathbf{x}, \sigma^2 \mathbf{I}) \Rightarrow \mathbf{y} = \mathbf{x} + \sigma \cdot \boldsymbol{\epsilon}, \boldsymbol{\epsilon} \sim \mathcal{N}(\mathbf{0}, \mathbf{I})$. For any ‘‘location-scale’’ family of distributions we can choose the standard distribution (with location = 0, scale = 1) as the auxiliary variable $\boldsymbol{\epsilon}$, and let $g(\cdot) = \text{location} + \text{scale} \cdot \boldsymbol{\epsilon}$. Examples: Laplace, Elliptical, Student’s t, Logistic, Uniform, Triangular and Gaussian distributions.
3. Implicit distributions. $q(\mathbf{y}|\mathbf{x})$ could be modeled by neural networks, which implies $\mathbf{y} = f(\mathbf{x}) + g(\boldsymbol{\epsilon}), \boldsymbol{\epsilon} \sim p(\boldsymbol{\epsilon})$, where f and g are one-to-one nonlinear transformations.

\square

B Derivations

Derivation of equality in JSD

$$\begin{aligned}
& JSD(p(\mathbf{y}, t), p_g(\mathbf{y}, t)) \\
&= \frac{1}{2} \mathcal{D}_{\text{KL}} \left[p(\mathbf{y}, t) \left\| \frac{p(\mathbf{y}, t) + p_g(\mathbf{y}, t)}{2} \right\| \right] + \frac{1}{2} \mathcal{D}_{\text{KL}} \left[p_g(\mathbf{y}, t) \left\| \frac{p(\mathbf{y}, t) + p_g(\mathbf{y}, t)}{2} \right\| \right] \\
&= \frac{1}{2} E_{\mathbf{y}, t \sim p(\mathbf{y}, t)} \left[\log \frac{2 \cdot p(\mathbf{y}, t)}{p(\mathbf{y}, t) + p_g(\mathbf{y}, t)} \right] + \frac{1}{2} E_{\mathbf{y}, t \sim p_g(\mathbf{y}, t)} \left[\log \frac{2 \cdot p_g(\mathbf{y}, t)}{p(\mathbf{y}, t) + p_g(\mathbf{y}, t)} \right] \\
&= \frac{1}{2} E_{t \sim p_\pi(t), \mathbf{y} \sim p(\mathbf{y} | t)} \left[\log \frac{2 \cdot p(\mathbf{y} | t) p_\pi(t)}{p(\mathbf{y} | t) p_\pi(t) + p_g(\mathbf{y} | t) p_\pi(t)} \right] \\
&\quad + \frac{1}{2} E_{t \sim p_\pi(t), \mathbf{y} \sim p_g(\mathbf{y} | t)} \left[\log \frac{2 \cdot p_g(\mathbf{y} | t) p_\pi(t)}{p(\mathbf{y} | t) p_\pi(t) + p_g(\mathbf{y} | t) p_\pi(t)} \right] \\
&= \mathbb{E}_{t \sim p_\pi(t)} \left[\frac{1}{2} E_{\mathbf{y} \sim p(\mathbf{y} | t)} \left[\log \frac{2 \cdot p(\mathbf{y} | t)}{p(\mathbf{y} | t) + p_g(\mathbf{y} | t)} \right] + \frac{1}{2} E_{\mathbf{y} \sim p_g(\mathbf{y} | t)} \left[\log \frac{2 \cdot p_g(\mathbf{y} | t)}{p(\mathbf{y} | t) + p_g(\mathbf{y} | t)} \right] \right] \\
&= \mathbb{E}_{t \sim p_\pi(t)} [JSD(p(\mathbf{y} | t), p_g(\mathbf{y} | t))].
\end{aligned}$$

C Limitations and social impacts

Limitations. Currently applying the diffusion-based noise injection does improve the general performance of GANs. However, when the training dataset size is very small, the improvement is only comparable to state-of-the-art domain-specific augmentation methods. The complementariness of our method with domain-specific augmentation is not clear at this moment and deserves further study. Moreover, current experiments are focused on image generation tasks with either the StyleGAN2 or ProjectedGAN framework. We leave the evaluation of our method with other GAN frameworks for future study.

Potential negative societal impacts. The major negative societal impacts for almost all generative models are generating fake images for malicious use, such as hate symbols and pornographics. Our Diffusion-GAN model is capable of generating high-fidelity images with only a small number of training samples. Then, if the training data contains violence, erotic samples or discrimination, our model could learn to generate these malicious images with limited data samples. Thus, how to prevent our model from being abused is a problem well worth careful investigation.

D Details of toy example

Here, we provide the detailed analysis of the JS divergence toy example.

Notation. Let \mathcal{X} be a compact metric set (such as the space of images $[0, 1]^d$) and $\text{Prob}(\mathcal{X})$ denote the space of probability measures defined on \mathcal{X} . Let \mathbb{P}_r be the target data distribution and \mathbb{P}_g ¹ be the generator distribution. The JSD between the two distributions $\mathbb{P}_r, \mathbb{P}_g \in \text{Prob}(\mathcal{X})$ is defined as:

$$\mathcal{D}_{\text{JS}}(\mathbb{P}_r || \mathbb{P}_g) = \frac{1}{2} \mathcal{D}_{\text{KL}}(\mathbb{P}_r || \mathbb{P}_m) + \frac{1}{2} \mathcal{D}_{\text{KL}}(\mathbb{P}_g || \mathbb{P}_m), \quad (12)$$

where \mathbb{P}_m is the mixture $(\mathbb{P}_r + \mathbb{P}_g)/2$ and \mathcal{D}_{KL} denotes the Kullback-Leibler divergence, i.e., $\mathcal{D}_{\text{KL}}(\mathbb{P}_r || \mathbb{P}_g) = \int_{\mathcal{X}} p_r(x) \log \left(\frac{p_r(x)}{p_g(x)} \right) dx$. More generally, f -divergence [Nowozin et al., 2016]

¹For notation simplicity, g and G both denote the generator network in GANs in this paper.

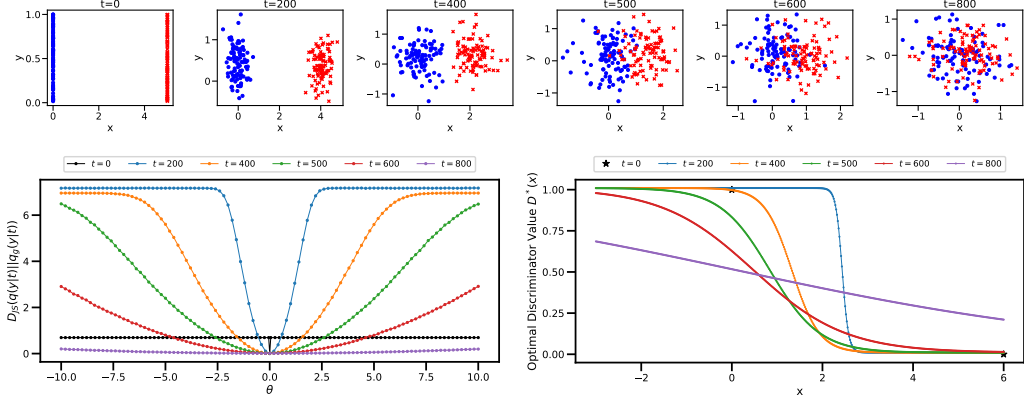


Figure 6: We show the data distribution and $\mathcal{D}_{JS}(\mathbb{P}_r || \mathbb{P}_g)$.

between \mathbb{P}_r and \mathbb{P}_g is defined as:

$$\mathcal{D}_f(\mathbb{P}_r || \mathbb{P}_g) = \int_{\mathcal{X}} p_g(\mathbf{x}) f\left(\frac{p_r(\mathbf{x})}{p_g(\mathbf{x})}\right) d\mathbf{x}, \quad (13)$$

where the generator function $f : \mathbb{R}_+ \rightarrow \mathbb{R}$ is a convex and lower-semicontinuous function satisfying $f(1) = 0$. We refer to Nowozin et al. [2016] for more details.

We recall the typical example introduced in Arjovsky and Bottou [2017] and follow the notations.

Example. Let $Z \sim U[0, 1]$ be the uniform distribution on the unit interval. Let $X \sim \mathbb{P}_r$ be the distribution of $(0, Z) \in \mathbb{R}^2$, which contains a 0 on the x-axis and a random variable Z on the y-axis. Let $X_g \sim \mathbb{P}_g$ be the distribution of $(\theta, Z) \in \mathbb{R}^2$, where θ is a single real parameter. In this case, the $\mathcal{D}_{JS}(\mathbb{P}_r || \mathbb{P}_g)$ is not continuous,

$$\mathcal{D}_{JS}(\mathbb{P}_r || \mathbb{P}_g) = \begin{cases} 0 & \text{if } \theta = 0, \\ \log 2 & \text{if } \theta \neq 0. \end{cases}$$

which can not provide a usable gradient for training. The derivation is as follows:

$$\begin{aligned} \mathcal{D}_{JS}(\mathbb{P}_r || \mathbb{P}_g) &= \frac{1}{2} \mathbb{E}_{x \sim p_r(x)} \left[\log \frac{2 \cdot p_r(x)}{p_r(x) + p_g(x)} \right] + \frac{1}{2} \mathbb{E}_{y \sim p_g(y)} \left[\log \frac{2 \cdot p_g(y)}{p_r(y) + p_g(y)} \right] \\ &= \frac{1}{2} \mathbb{E}_{x_1=0, x_2 \sim U[0,1]} \left[\log \frac{2 \cdot \mathbf{1}[x_1=0] \cdot U(x_2)}{\mathbf{1}[x_1=0] \cdot U(x_2) + \mathbf{1}[x_1=\theta] \cdot U(x_2)} \right] \\ &\quad + \frac{1}{2} \mathbb{E}_{y_1=\theta, y_2 \sim U[0,1]} \left[\log \frac{2 \cdot \mathbf{1}[y_1=\theta] \cdot U(y_2)}{\mathbf{1}[y_1=0] \cdot U(y_2) + \mathbf{1}[y_1=\theta] \cdot U(y_2)} \right] \\ &= \frac{1}{2} \left[\log \frac{2 \cdot \mathbf{1}[x_1=0]}{\mathbf{1}[x_1=0] + \mathbf{1}[x_1=\theta]} \Big|_{x_1=0} \right] + \frac{1}{2} \left[\log \frac{2 \cdot \mathbf{1}[y_1=\theta]}{\mathbf{1}[y_1=0] + \mathbf{1}[y_1=\theta]} \Big|_{y_1=\theta} \right] \\ &= \begin{cases} 0 & \text{if } \theta = 0, \\ \log 2 & \text{if } \theta \neq 0. \end{cases} \end{aligned}$$

Although this simple example features distributions with disjoint supports, the same conclusion holds when the supports have a non empty intersection contained in a set of measure zero [Arjovsky and Bottou, 2017]. This happens to be the case when two low dimensional manifolds intersect in general position [Arjovsky and Bottou, 2017]. To avoid the potential issue caused by having non-overlapping distribution supports, a common remedy is to use Wasserstein-1

distance which in theory can still provide usable gradient [Arjovsky and Bottou, 2017, Arjovsky et al., 2017]. In this case, the Wasserstein-1 distance is $|\theta|$.

Diffusion-based noise injection In general, with our diffusion noise injected, we could have,

$$\begin{aligned} p_{r',t} &= \int_{\mathcal{X}} p_r(\mathbf{x}) \mathcal{N}(\mathbf{y}; \sqrt{\bar{\alpha}_t} \mathbf{x}, (1 - \bar{\alpha}_t) \sigma^2 \mathbf{I}) d\mathbf{x} \\ p_{g',t} &= \int_{\mathcal{X}} p_g(\mathbf{x}) \mathcal{N}(\mathbf{y}; \sqrt{\bar{\alpha}_t} \mathbf{x}, (1 - \bar{\alpha}_t) \sigma^2 \mathbf{I}) d\mathbf{x} \\ \mathcal{D}_{JS}(p_{r',t} || p_{g',t}) &= \frac{1}{2} \mathbb{E}_{p_{r',t}} \left[\log \frac{2p_{r',t}}{p_{r',t} + p_{g',t}} \right] + \frac{1}{2} \mathbb{E}_{p_{g',t}} \left[\log \frac{2p_{g',t}}{p_{r',t} + p_{g',t}} \right] \end{aligned}$$

For the previous example, we have Y'_t and $Y'_{g,t}$ such that,

$$Y'_t = (y_1, y_2) \sim p_{r',t} = \mathcal{N}(y_1 | 0, b_t) f(y_2), Y'_{g,t} = (y_{g,1}, y_{g,2}) \sim p_{g',t} = \mathcal{N}(y_{g,1} | a_t \theta, b_t) f(y_{g,2}),$$

where $f(\cdot) = \int_0^1 \mathcal{N}(\cdot | a_t Z, b_t) U(Z) dZ$, a_t and b_t are abbreviations for $\sqrt{\bar{\alpha}_t}$ and $(1 - \bar{\alpha}_t) \sigma^2$. The supports of Y'_t and $Y'_{g,t}$ are both the whole metric space \mathbb{R}^2 and they overlap with each other depending on t , as shown in Figure 6. As t increases, the high density region of Y'_t and $Y'_{g,t}$ get closer since the weight a_t is decreasing towards 0. Then, we derive the JS divergence,

$$\begin{aligned} \mathcal{D}_{JS}(p_{r',t} || p_{g',t}) &= \frac{1}{2} \mathbb{E}_{y_1 \sim \mathcal{N}(y_1 | 0, b_t), y_2 \sim f(y_2)} \left[\log \frac{2 \cdot \mathcal{N}(y_1 | 0, b_t) f(y_2)}{\mathcal{N}(y_1 | 0, b_t) f(y_2) + \mathcal{N}(y_1 | a_t \theta, b_t) f(y_2)} \right] \\ &\quad + \frac{1}{2} \mathbb{E}_{y_{g,1} \sim \mathcal{N}(y_{g,1} | 0, b_t), y_{g,2} \sim f(y_{g,2})} \left[\log \frac{2 \cdot \mathcal{N}(y_{g,1} | a_t \theta, b_t) f(y_{g,2})}{\mathcal{N}(y_{g,1} | 0, b_t) f(y_{g,2}) + \mathcal{N}(y_{g,1} | a_t \theta, b_t) f(y_{g,2})} \right] \\ &= \frac{1}{2} \mathbb{E}_{y_1 \sim \mathcal{N}(0, b_t)} \left[\log \frac{2 \cdot \mathcal{N}(y_1 | 0, b_t)}{\mathcal{N}(y_1 | 0, b_t) + \mathcal{N}(y_1 | a_t \theta, b_t)} \right] \\ &\quad + \frac{1}{2} \mathbb{E}_{y_{g,1} \sim \mathcal{N}(a_t \theta, b_t)} \left[\log \frac{2 \cdot \mathcal{N}(y_{g,1} | a_t \theta, b_t)}{\mathcal{N}(y_{g,1} | 0, b_t) + \mathcal{N}(y_{g,1} | a_t \theta, b_t)} \right] \end{aligned}$$

which is clearly continuous and differentiable.

We show this $\mathcal{D}_{JS}(p_{r',t} || p_{g',t})$ with respect to increasing t values and a θ grid in the second row of Figure 6. As shown in the left panel, the black line with $t = 0$ shows the original JSD, which is not even continuous, while as the diffusion level t increments, the lines become smoother and flatter. It is clear to see that these smooth curves provide good learning signals for θ . Recall that the Wasserstein-1 distance is $|\theta|$ in this case. Meanwhile, we could observe with an intense diffusion, *e.g.*, $t = 800$, the curve becomes flatter, which indicates smaller gradients and a much slower learning process. This motivates us that an adaptive diffusion could provide different level of gradient smoothness and is possibly better for training. The right panel shows the optimal discriminator outputs over the space \mathcal{X} . With diffusion, the optimal discriminator is well defined over the space and the gradient is smooth, while without diffusion the optimal discriminator is only valid on two star points. Interestingly, we find that smaller t drives the optimal discriminator to become more assertive while larger t makes discriminator become more neutral. The diffusion here works like a scale to balance the power of the discriminator.

E Dataset descriptions

The CIFAR-10 dataset consists of 50k 32×32 training images in 10 categories. The STL-10 dataset originated from ImageNet [Deng et al., 2009] consists of 100k unlabeled images in 10 categories, and we resize them to 64×64 resolution. For LSUN datasets, we sample 200k

images from LSUN-Bedroom, use the whole 125k images from LSUN-Church, and resize them to 256×256 resolution for training. The AFHQ datasets includes around 5k 512×512 images per category for dogs, cats, and wild life; we train a separate network for each of them and also train a network for all of them, denoted as AFHQ-All, for comparison. The FFHQ contains 70k images crawled from Flickr at 1024×1024 resolution and we use all of them for training.

F Algorithm

We provide the Diffusion-GAN algorithm in Algorithm 1.

Algorithm 1 Diffusion-GAN

```

while  $i \leq$  number of training iterations do
  Step I: Update discriminator
  • Sample minibatch of  $m$  noise samples  $\{z_1, z_2, \dots, z_m\} \sim p_z(z)$ .
  • Obtain generated samples  $\{x_{g,1}, x_{g,2}, \dots, x_{g,m}\}$  by  $x_g = G(z)$ .
  • Sample minibatch of  $m$  data examples  $\{x_1, x_2, \dots, x_m\} \sim p(x)$ .
  • Sample  $\{t_1, t_2, \dots, t_m\}$  from  $t_{epl}$  list uniformly with replacement.
  • For  $j \in \{1, 2, \dots, m\}$ , sample  $y_j \sim q(y_j|x_j, t_j)$  and  $y_{g,j} \sim q(y_{g,j}|x_{g,j}, t_j)$ 
  • Update discriminator by maximizing Equation (8).

  Step II: Update generator
  • Sample minibatch of  $m$  noise samples  $\{z_1, z_2, \dots, z_m\} \sim p_z(z)$ 
  • Obtain generated samples  $\{x_{g,1}, x_{g,2}, \dots, x_{g,m}\}$  by  $x_g = G(z)$ .
  • Sample  $\{t_1, t_2, \dots, t_m\}$  from  $t_{epl}$  list with replacement.
  • For  $j \in \{1, 2, \dots, m\}$ , sample  $y_{g,j} \sim q(y_{g,j}|x_{g,j}, t_j)$ 
  • Update generator by minimizing Equation (8).

  Step III: Update diffusion
  if  $i \bmod 4 == 0$  then
    Update  $T$  by Equation (10)
    Sample  $t_{epl} = [0, \dots, 0, t_1, \dots, t_{32}]$ , where  $t_k \sim p_\pi$  for  $k \in \{1, \dots, 32\}$ .  $p_\pi$  is in Equation (11).  $\{t_{epl}$  has 64 dimensions.}
  end if
end while

```

G Hyperparameters

Diffusion-GAN introduces a new hyperparameter d_{target} , which is a threshold to identify whether the current discriminator is overfitting. We find StyleGAN2 based models are not sensitive to the values of d_{target} , so we set $d_{target} = 0.6$ for them across all datasets. We report d_{target} of Diffusion ProjectedGAN for our experiments in Table 2. Overall, we didn’t modify anything in the model architectures and training hyperparameters, such as learning rate and batch size. The forward diffusion configuration and model training configurations are as follows.

Diffusion config. For our diffusion-based noise injection, we set up a linearly increasing schedule for β_t , where $t \in \{1, 2, \dots, T\}$. For pixel level injection in StyleGAN2, we follows [Ho et al., 2020] and set $\beta_0 = 0.0001$ and $\beta_T = 0.02$. We adaptively modify T ranging from $T_{\min} = 5$ to $T_{\max} = 1000$. The image pixels are usually rescaled to $[-1, 1]$ so we set the Gaussian noise standard deviation $\sigma = 0.05$. For feature level injection in Diffusion ProjectedGAN, we

Datasets	r_d
CIFAR-10 (32×32 , 50k images)	0.45
STL-10 (64×64 , 100k images)	0.6
LSUN-Church (256×256 , 120k images)	0.2
LSUN-Bedroom (256×256 , 200k images)	0.2

Table 2: d_{target} for Diffusion ProjectedGAN

Diffusion config for pixel	$\beta_0 = 0.0001, \beta_T = 0.02, T_{\min} = 5, T_{\max} = 1000, \sigma = 0.05$
Diffusion config for feature	$\beta_0 = 0.0001, \beta_T = 0.01, T_{\min} = 5, T_{\max} = 500, \sigma = 0.5$

Table 3: Diffusion config.

set $\beta_0 = 0.0001, \beta_T = 0.01, T_{\min} = 5, T_{\max} = 500$ and $\sigma = 0.5$. We list all these values in Table 3

Model config. For StyleGAN2 based models, we borrow the config settings provided by Karras et al. [2020a], which includes [‘auto’, ‘stylegan2’, ‘cifar’, ‘paper256’, ‘paper512’, ‘stylegan2’]. We create the ‘stl’ config based on ‘cifar’ with a small modification that we change the gamma term to be 0.01. For ProjectedGAN models, we use the recommended default config [Sauer et al., 2021], which is based on FastGAN. We report the config settings that we used for our experiments in Table 4.

H More generated images

We provide more generated images for LSUN-Bedroom, LSUN-Church, AFHQ, and FFHQ datasets in Figure 7, Figure 8, and Figure 9.

I Implementation details

We implement an additional diffusion sampling pipeline, where the diffusion configurations are set in Appendix G. The T in the forward diffusion process is adaptively adjusted and clipped to $[T_{\min}, T_{\max}]$. As illustrated in Algorithm 1, at each update step, we sample t from t_{epl} for each data point \mathbf{x} , and then use the analytic Gaussian distribution at diffusion step t to sample \mathbf{y} . Next, we use \mathbf{y} and t instead of \mathbf{x} for optimization.

Diffusion StyleGAN2. We inherit all the network architectures from StyleGAN2 implemented by Karras et al. [2020a]. We modify the original mapping network, which is there for label conditioning and unused for unconditional image generation tasks, inside the discriminator to inject t . Specifically, we change the original input of mapping network, the class label c , to our discrete value timestep t . Then, we train the generator and discriminator with diffused samples \mathbf{y} and t .

Diffuson ProjectedGAN. To simplify the implementation and minimize the modifications to ProjectedGAN, we construct the discriminator as $D_\phi(\mathbf{y})$, where t is ignored. Our method is plugged in as a data augmentation method. The only change in the optimization stage is that the discriminator is fed with diffused images \mathbf{y} instead of original images \mathbf{x} .

Complementariness. We combine our method with other domain-specific augmentations by first applying their augmentation and then applying our forward diffusion.

Dataset	Models	Config	Specification
CIFAR-10 (32×32)	StyleGAN2	cifar	-
	StyleGAN2 + Diffaug	cifar	-
	StyleGAN2 + ADA	cifar	-
	Diffusion StyleGAN2	cifar	diffusion-pixel
	Diffusion StyleGAN2 + Diffaug	cifar	diffusion-pixel
	Diffusion StyleGAN2 + ADA	cifar	diffusion-pixel, ada-maxp=0.25
	ProjectedGAN	default	diffusion-feature
STL-10 (64×64)	StyleGAN2	stl	-
	StyleGAN2 + Diffaug	stl	-
	StyleGAN2 + ADA	stl	-
	Diffusion StyleGAN2	stl	diffusion-pixel
	Diffusion StyleGAN2 + Diffaug	stl	diffusion-pixel
	Diffusion StyleGAN2 + ADA	stl	diffusion-pixel, ada-maxp=0.25
	ProjectedGAN	default	diffusion-feature
LSUN-Bedroom (256×256)	StyleGAN2	paper256	-
	StyleGAN2 + Diffaug	paper256	-
	StyleGAN2 + ADA	paper256	-
	Diffusion StyleGAN2	paper256	diffusion-pixel
	Diffusion StyleGAN2 + Diffaug	paper256	diffusion-pixel
	Diffusion StyleGAN2 + ADA	paper256	diffusion-pixel, ada-maxp=0.1
	ProjectedGAN	default	diffusion-feature
LSUN-Church (256×256)	StyleGAN2	paper256	-
	StyleGAN2 + Diffaug	paper256	-
	StyleGAN2 + ADA	paper256	-
	Diffusion StyleGAN2	paper256	diffusion-pixel
	Diffusion StyleGAN2 + Diffaug	paper256	diffusion-pixel
	Diffusion StyleGAN2 + ADA	paper256	diffusion-pixel, ada-maxp=0.25
	ProjectedGAN	default	diffusion-feature
AFHQ-All (512×512)	StyleGAN2	paper512	-
	StyleGAN2 + Diffaug	paper512	-
	StyleGAN2 + ADA	paper512	-
	Diffusion StyleGAN2	paper512	diffusion-pixel
	Diffusion StyleGAN2 + Diffaug	paper512	diffusion-pixel
	Diffusion StyleGAN2 + ADA	paper512	diffusion-pixel, ada-maxp=0.1
	FFHQ (1024×1024)	StyleGAN2	paper1024
StyleGAN2 + Diffaug		paper1024	-
StyleGAN2 + ADA		paper1024	-
Diffusion StyleGAN2		paper1024	diffusion-pixel
Diffusion StyleGAN2 + Diffaug		paper1024	diffusion-pixel
Diffusion StyleGAN2 + ADA		paper1024	diffusion-pixel, ada-maxp=0.25

Table 4: The config setting of StyleGAN2 based models and ProjectedGAN based models. For StyleGAN2 based models, we borrow the config settings provided by Karras et al. [2020a], which includes [‘auto’, ‘stylegan2’, ‘cifar’, ‘paper256’, ‘paper512’, ‘paper1024’]. We create the ‘stl’ config based on ‘cifar’ with small modifications that we change the gamma term to be 0.01. For ProjectedGAN models, we use the recommended default config [Sauer et al., 2021], which is based on FastGAN.

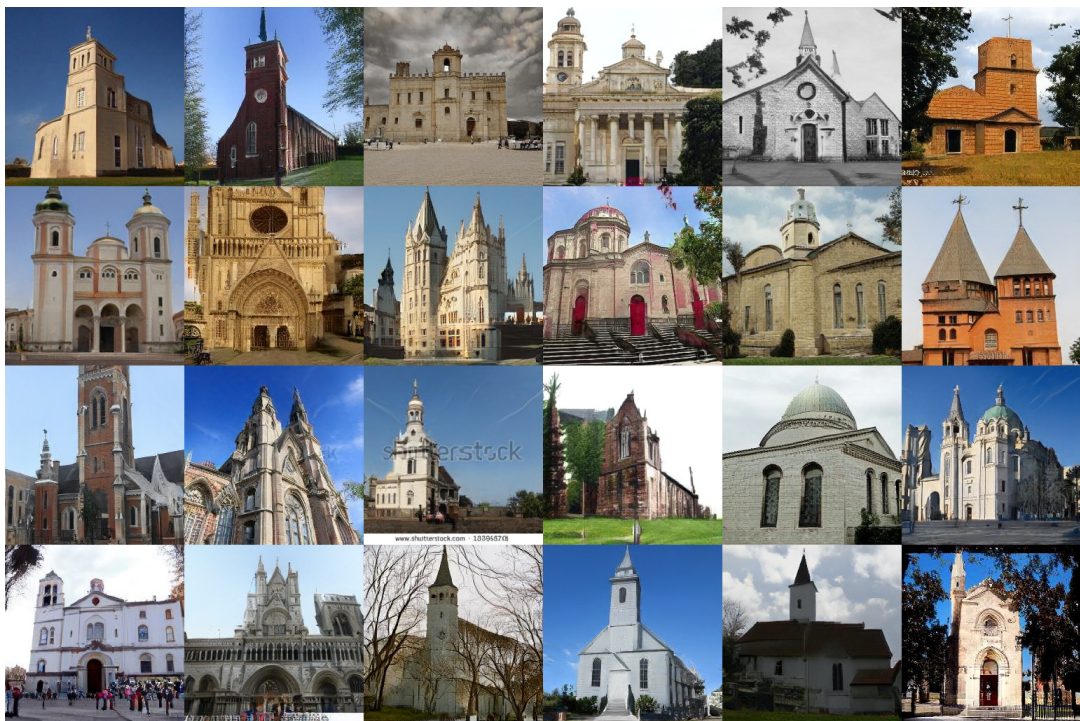
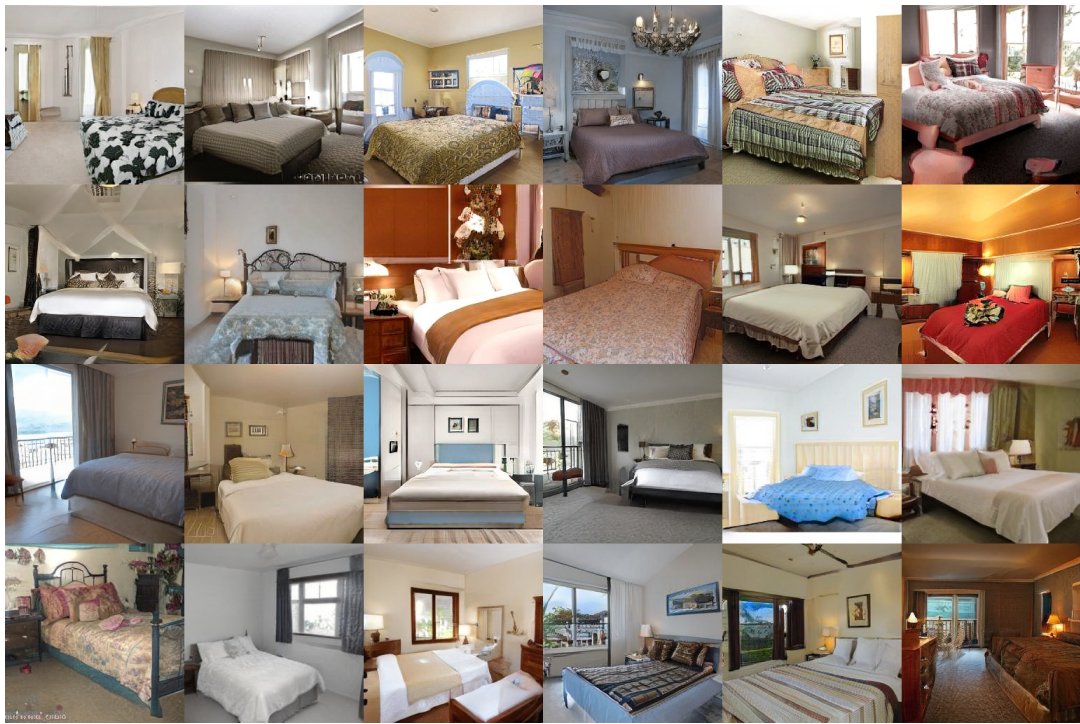


Figure 7: More generated images for LSUN-Bedroom (FID 1.43, Recall 0.58) and LSUN-Church (FID 1.85, Recall 0.65) from Diffusion ProjectedGAN.



Figure 8: More generated images for AFHQ-All from Diffusion StyleGAN2 (FID 4.93, Recall 0.34).



Figure 9: More generated images for FFHQ from Diffusion StyleGAN2 (FID 3.71, Recall 0.43).